THE DIFFUSION OF HYDROGEN IN IRON AND STEEL

By

STEVEN EDWARD MASCHINO

Bachelor of Science in Mechanical Engineering

Oklahoma State University

Stillwater, Oklahoma

1981

Submitted to the Faculty of the Graduate College
of the Oklahoma State University
in partial fulfillment of the requirements
for the Degree of
MASTER OF SCIENCE
December, 1982

THE DIFFUSION OF HYDROGEN IN

IRON AND STEEL

Thesis Approved:

J. Thesis Adviser

C E Price

R L Fowery

Norman N Durham

Dean of the Graduate College

ACKNOWLEDGMENTS

The author wishes to express his deepest appreciation to his major adviser, Dr. J. Murali, whose guidance, criticism and overall support was instrumental in the successful completion of this thesis. Gratitude is also extended to Dr. C. E. Price and Dr. Richard Lowery of the committee who provided many helpful suggestions.

The financial support in the form of teaching assistantships from the Mechanical Engineering Department, Oklahoma State University, from June 1981-July 1982, is acknowledged with gratitude.

The Armco iron used in the study was supplied by Jerry Arnold and his generosity is appreciated.

Finally, special gratitude is expressed to the author's wife, Tamara, for her devotion, encouragement, and many sacrifices.

TABLE OF CONTENTS

LIST OF TABLES

LIST OF FIGURES

CHAPTER I

INTRODUCTION

A. The Importance of Hydrogen

The damaging effects of hydrogen on the mechanical properties of steels is well documented, but not thoroughly understood. Under certain conditions, hydrogen can permeate steels and induce partial or complete brittleness. The knowledge of how hydrogen interacts with steels is important to many sectors of industry which use these alloys in environments where hydrogen-induced failure is a likely occurrence.

Hydrogen usage in many industrial processes has increased. Current U.S. hydrogen energy consumption is about 1.05×10^{18} J/yr (1). Processes which use hydrogen as an important feedstock include refining petroleum, hydrogenating vegetable oils, synthesizing chemicals and for the manufacture of semiconductors. Several studies (2), (3), (4) have addressed the possibilities of utilizing hydrogen in gaseous form for space heating and electricity generation. Hydrogen could also be used as a gaseous or liquid fuel road transportation and as a liquid fuel in air transportation. Vehicles have been operated using hydrogen gas as a fuel that was stored by metal hydrides (2). Metal hydrides are metallic compounds which react under certain conditions with a large volume of hydrogen gas and hold it through weak bonds in a solid or powdery form. One problem associated with using metal hydrides for hydrogen storage concerns their weight. Presently, metal hydrides and their storage containers are too

large and too heavy for implementation in commercial vehicles. In many of the studies (2), (3), (4) on hydrogen utilization, it has been emphasized that the technical problems of hydrogen use as an energy carrier could be solved, making hydrogen an economically attractive fuel.

Hydrogen is also technically important due to the fact that it is present in corrosion reactions. Hydrogen can be generated by the corrosion reaction of a metal with aqueous environments such as water, moist air, acids and hydrocarbons. Sulfides that are dissolved in moisture on a steel structure can promote hydrogen entry into the steel during a corrosion reaction by acting as a hydrogen recombination poison. Collapse of Point Pleasant (5), West Virginia, bridge, began by failure of a 1060 steel eyebar. Sulfur compounds found on the fracture surface are believed to have played an important role in the crack growth in the eyebar.

The extensive hydrogen storage and transmission systems required for implementation of the hydrogen economy must operate safely, reliably and economically for long periods of time. It is necessary for economic reasons to use materials which are not susceptible to the adverse affects of hydrogen. Therefore, the design, fabrication and operation of these hydrogen systems requires a thorough understanding and consideration of all aspects of hydrogen embrittlement.

B. Hydrogen Embrittlement

Hydrogen embrittlement is a general term which refers to mechanical degradation of a metal caused by the presence of, or interaction with, hydrogen. Hydrogen embrittlement has been classified into three different types that may be interrelated but have different embrittlement

characteristics. ASTM STP 543 (6) gives these types as:

1. Internal reversible hydrogen embrittlement (IHE).
2. Hydrogen environment embrittlement (HEE).
3. Hydrogen reaction embrittlement (HRE).

Internal reversible hydrogen embrittlement is a type of embrittlement that is due to hydrogen that has been absorbed into the metal. The most widely recognized example of this type of degradation is the delayed failure of hydrogen-charged high strength steels. The absorption of hydrogen by the metal can occur during plating or direct contact with gaseous hydrogen or as the result of chemical reaction of the metal with water or other hydrogen containing species. Hydrogen absorption can occur during melting, casting, pickling and welding operations. Hydrogen can also be present due to the corrosion of steel in certain aqueous environments. In acid environments, the corrosion reactions might be the following:

the dissolution of iron, $Fe \rightarrow Fe^{++} + 2e^{-}$ (anodic reaction)

and hydrogen evolution, $2H^{+} + 2e^{-} \rightarrow 2H$ (cathodic reaction)

The hydrogen atoms which are produced at the steel surface may recombine to form H_2 or may be absorbed by the steel as atomic hydrogen. The absorption of hydrogen in the gas phase will be increased by increased temperatures and pressure. For a given concentration of absorbed hydrogen, IHE is most severe in the vicinity of room temperature (7).

Normally, for IHE to occur, the hydrogen must be concentrated at specific embrittlement locations such as in the plastic zones of cracks, dislocations, particle-matrix, interfaces, etc. Because of the time required for hydrogen to diffuse to embrittlement sites, delayed failure of the steel is characteristic of this type of hydrogen damage. This

time dependent nature suggests that the diffusion of hydrogen within the lattice controls this type of embrittlement (6). IHE is reversible in that, if microscopic cracks have not been formed and if the hydrogen is removed from the metal, there is no embrittlement.

Hydrogen environment embrittlement is used to signify the degradation of mechanical properties of a metal, which occurs while the metal is exposed to a hydrogen environment (7). HEE was recognized as a serious problem in the mid 1960s when the National Aeronautics and Space Administration (NASA) and its contractors experienced failure of ground based hydrogen storage tanks (8). These tanks were rated for hydrogen pressures of 35 to 70 MN/m^2. This type of degradation is most severe at room temperature and it affects high-strength structural alloys such as steels and nickel-base alloys (6). The processes that take place in gaseous hydrogen embrittlement are the transport of the hydrogen gas to the metal surface, adsorption onto the metal surface, dissociation to atomic hydrogen and transport of atomic hydrogen into the matrix to the region where embrittlement will take place (9). The details involved during the adsorption and dissociation process are controversial. Frandsen and Marcus (9) suggested several possible steps for this process which are as follows:

1. The initial impingement of hydrogen gas onto the metal substrate; then either steps 2 or 3 might occur.
2. The physical adsorption of the moleculer hydrogen on the metal surface. "The physisorption process involves low energy Van der Waals bonds with no exchange of electrons" (9, p. 234).
3. The molecular chemisorption of the molecular hydrogen on the metal surface. "In this process the hydrogen bond length is

extended and partial electron transfer takes place between the hydrogen molecule and the metal substrate" (9, p. 234). The energy for chemisorption is generally greater than that of physisorption with the exception that impurities species might lower the binding energy for chemisorption.

4. The next phase of the absorption process is the complete dissociation of the absorbed molecule to atomic hydrogen. "This step might be preceded by the need for surface diffusion of the adsorbed molecule to a more active site for complete dissociation" (9, p. 234).

Hydrogen reaction embrittlement results when a chemical reaction occurs between hydrogen and the metal or some constituent in the metal to cause a marked deterioration in mechanical properties. Three examples (6) of this type of hydrogen damage are:

1. The reaction of hydrogen with carbon in steels to form methane.
2. The reaction of hydrogen with copper oxide in copper alloys to form water or steam.
3. The reaction of hydrogen with the matrix or an alloying element to form a hydride.

The source of hydrogen atoms for these embrittling reactions can be the dissociation of molecular hydrogen under conditions of high hydrogen partial pressures (500-2500 psi) and high temperatures (400-800^{o}C). These conditions are met in hydrogenation processes and in high temperature steam production. When methane gas or steam forms in the metal, it tends to settle into voids or cracks at very high pressures, 10^{4}MPA (10), thus embrittling the metal by forcing the crack apart and extending it. This type of damage is of considerable concern to the petroleum and

chemical industries and extensive investigation have led to the development of the well-known Nelson diagrams (11) which delineate the safe hydrogen pressure-temperature conditions of operations for various steels. HRE is essentially a permanent, irreversible embrittlement, and increased temperatures and pressures increase the rates of reaction and thus the tendency toward this type of embrittlement (7).

It is clear from the above that in every classification of hydrogen embrittlement the degradation of a metal depends on the transport reactions involved in moving the hydrogen from its source to the locations where it reacts with the metal. The rate at which hydrogen diffuses to the embrittlement sites is also important. Hydrogen diffuses through metals in atomic form and since it is the smallest of all atoms, its diffusivity is orders of magnitude greater than that of any other solute (12). The study of hydrogen transport reactions are an integral part of hydrogen embrittlement analysis.

The degree to which hydrogen is delayed or trapped in the metal as it diffuses is closely related to the resistance or susceptibility of steel to hydrogen embrittlement. Hydrogen trapping sites that have been identified in iron, steel and other metals include dislocation, vacancies, voids, grain boundaries and particle-matrix interfaces (13). Even though these trapping sites are known to effect hydrogen diffusion in steel, there is still a considerable lack of understanding in the details of hydrogen trapping. McNabb and Foster's mathematical model (14) and Oriani's physical model of trapping (15) are among several important developments that have led to improvements in the understanding of hydrogen trapping behavior in steels. With these models it is possible to determine various trapping characteristics such as hydrogen-trap binding

energy, trap density, trap capture and release rates and other parameters. A model which considers the effects of hydrogen trapping and their relationship to hydrogen damage of steel and other metals is the trap theory of hydrogen embrittlement (16). Effective utilization of models that predict hydrogen embrittlement behaviors in steels cannot be attained until a better understanding of various trapping characteristics and hydrogen transport mechanisms are better understood.

C. Purpose

The purpose of this thesis was to analyze hydrogen diffusion and trapping behavior in Armco iron and 1015 steel. The Armco iron and 1015 steel were chosen to demonstrate the influence of minor alloy additions; i.e., carbon, on reversible trapping behavior. The materials were tested in the annealed and cold worked condition so that the effect of mechanical deformation on trapping could be analyzed. A sensitive electrochemical hydrogen detection technique was used to obtain hydrogen permeation data from which various trapping parameters and diffusivities were determined. A computer program was developed to analyze permeation transients and to determine trapping characteristics. This program was based on a numerical solution (17) to a mathematical formulation (14) of hydrogen trapping reactions.

CHAPTER II

LITERATURE SURVEY

A. Diffusion and Trapping

Hydrogen diffusion in steel is a process by which hydrogen is transported through steel, for instance, by interstitial jumps through the lattice (16). Fick's laws can be used to describe homogeneous diffusion of hydrogen in iron and steel under conditions in which lattice defects or traps have a negligible delaying effect on the diffusing hydrogen. Fick's laws for one dimensional diffusion are:

$$\text{First Law:} \quad J = -D \frac{\partial c}{\partial x} \tag{1}$$

$$\text{Second Law:} \quad \frac{\partial c}{\partial t} = D \frac{\partial^2 c}{\partial x^2} \tag{2}$$

where

C = concentration of the diffusing species

J = flux of the diffusing species across a reference plane perpendicular to the x axis

D = diffusion coefficient

Fick's first law states, in this case, that when there is a concentration gradient of a diffusing substance along the x axis, the flux is proportional to the concentration gradient. Fick's second law describes the concentration changes of the diffusing species within the volume during the diffusing process. Solutions to Fick's laws, subject to various initial and boundary conditions, are given by Crank (18).

The diffusion coefficient, D, in the above equation is related to temperature by the following expression:

$$D = D_o \exp -Q/RT \qquad (3)$$

where

D = diffusion coefficient

D_o = pre-exponential term or frequency factor

Q = activation energy for diffusion

R = universal gas constant

T = temperature, ^oK

The equation for diffusivity of hydrogen in iron at high temperatures (300-700^{o}C), has been shown (19) to yield a straight line when the log of the diffusion coefficients are plotted against the reciprocal of the absolute temperature. However, experimental values of diffusivity vary considerably, especially in the vicinity of room temperatures where the values are scattered over several orders of magnitude. Volkl and Alefeld (19) have compiled the results of forty-six studies on the diffusion of hydrogen in iron and their results are depicted in Figure 1. The curve marked D_1 on the figure is one derived by Volkl and Alefeld (19) which is the upper limit of several sets of measured data and, as they discussed, is probably descriptive of pure diffusion in iron. This curve is described by the relation:

$$D_1 = 4 \times 10^{-4} \exp ((-1100 \text{ cal/mol/RT}) \text{ cm}^2/\text{s}. \qquad (4)$$

Volkl and Alefeld (19) also defined an expression for the hydrogen diffusion coefficient which fits a large amount of data and is given by D_2:

$$D_2 = 7.5 \times 10^{-4} \exp ((-1900 \text{ cal/mol/RT}) \text{ cm}^2/\text{s}. \qquad (5)$$

It is interesting to note that Equation 5 is very similar to the equation

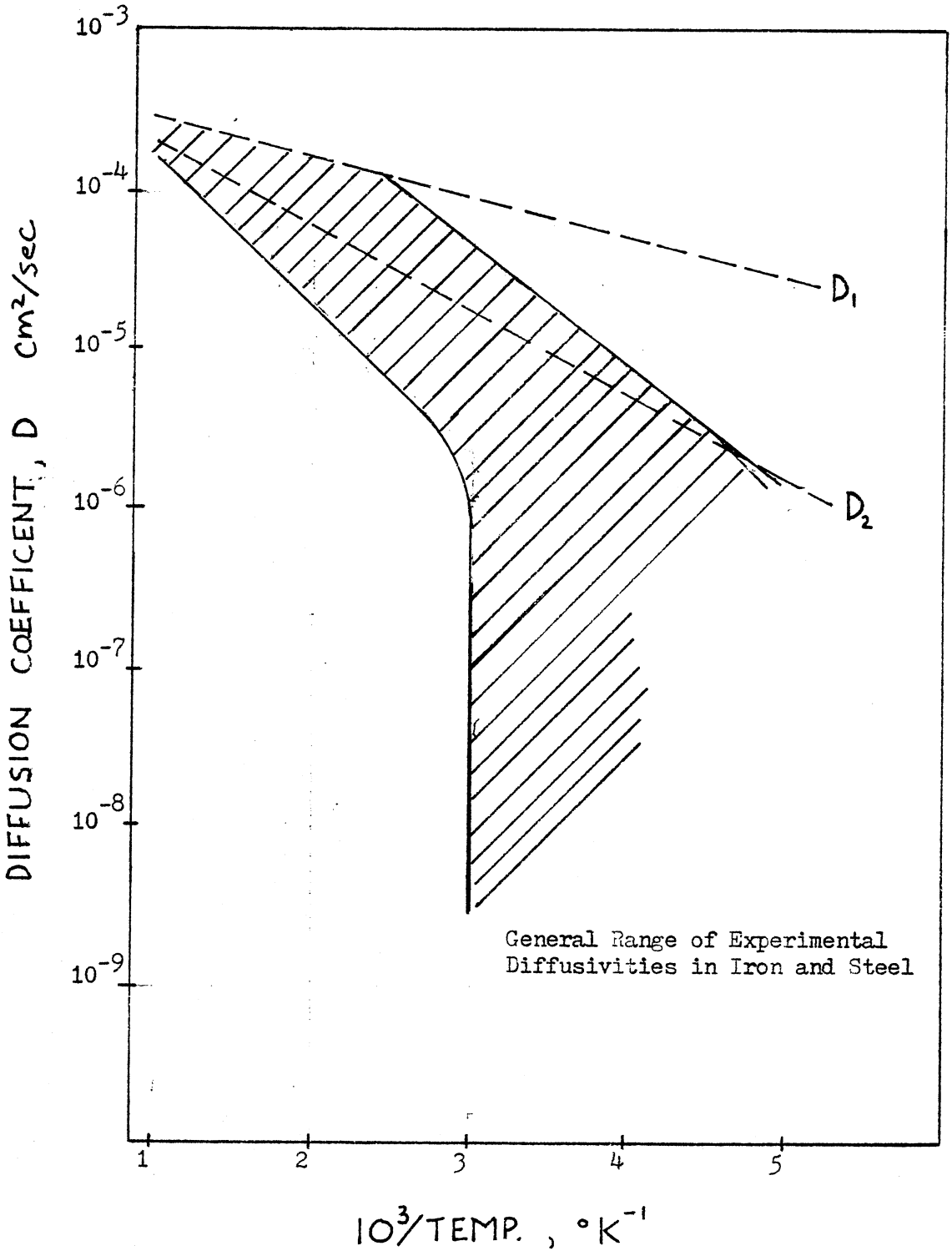

Figure 1. Range of Values for the Diffusivity of Hydrogen in Iron.

of diffusivity given by Oriani (15) from the results of Gonzalez's analysis (20) of steady state permeability data. Oriani's equation is given is as:

$$D = 7.8 \times 10^{-4} \exp ((-1900 \text{ cal/mol/RT}) \text{ cm}^2/\text{s}. \quad (6)$$

Generally, the above equations do not describe diffusion of hydrogen in iron or steel near room temperature. When traps are present in a material, some of the diffusing hydrogen tends to become immobilized and there is an exchange of hydrogen between traps and lattice sites. Trapping reactions effectively increase the activation energy for hydrogen diffusion. At high temperatures (400-800^{o}C), thermal energy decreases the effects of trapping and diffusion proceeds more like lattice diffusion.

Darken and Smith (21), in 1949, were first to report experimental evidence of hydrogen trapping in 4340 steel. They found that the solubility of hydrogen in cold worked steel was higher than that of annealed steel. This effect was suggested to be attributed to lattice imperfections in the iron lattice as caused by the cold working of the steel. The authors also found that hydrogen diffused into a specimen faster than it effused from the specimen, being initially saturated under the same boundary concentrations. These results suggested that Fick's second law which describes ordinary diffusion must be replaced by a nonlinear system of diffusion which would account for various trapping mechanisms.

B. Trapping Models

Several models have been proposed which deal with the nature of different types of traps and their interaction with hydrogen. McNabb and Foster (14) have developed a mathematical formulation that accounts for

the interchange of hydrogen between the diffusing and trapped populations. In their model, Fick's laws are modified on the assumption that hydrogen is delayed at fixed sites in the lattice. In addition, McNabb and Foster have categorized traps according the the tenacity with which they hold a captured atom. Those in the first category are reversible traps which have a negligible delaying effect, while those in the second category are irreversible traps where the captive hydrogen can no longer take place in the diffusion process over the time intervals and temperatures being considered. The third type of traps are all the remaining traps. These traps are considered active traps. McNabb and Foster assumed that one active trap can capture and release only one hydogren atom at a time and that the active traps can be described in their overall effect by two parameters, p and k. These authors postulated that the release probability, p, would be dependent on the temperature and nature of the active trap, but independent of the local concentrations of trapped and diffusing atoms. The theory also assumes that there is a uniform concentration of reversible traps and that these traps are saturable; i.e., have a finite capacity for hydrogen. The McNabb-Foster equations for transport are:

$$\frac{\partial c}{\partial t} + N \frac{\partial n}{\partial t} = D \nabla^2 C \tag{7}$$

$$\frac{\partial n}{\partial t} = kC(1-n) - pn \tag{8}$$

where

C = concentration of diffusible atoms

N = trap density

n = fractional occupancy of traps

D = lattice diffusivity

k = transition probability for hydrogen transport from lattice site to trap

p = transition probability for hydrogen escape from tap to lattice site

McNabb and Foster also described solutions of the diffusivity equation for various conditions of trapping. Their equation for the effective or experimental diffusivity, D_{eff}, in terms of the lattice diffusivity constant, D, is the following:

$$D_{eff} = D(1 + Nk/p)^{-1} \quad (9)$$

Equation 9 is based on the assumption that the traps present in the material are sparingly occupied and that the effective diffusivity does not depend on lattice concentration. Johnson et al., (22) expect the type of behavior denoted by Equation 9 to be encountered at low lattice concentrations and/or at temperatures rather high (50-700^{o}C) in the trapping regime. Thermal emptying of traps should produce low trap occupancy and give a linear coverage of trap concentration proportional to the lattice concentration.

The McNabb-Foster analysis is based on the a priori assumption that during a diffusion process any irreversible traps present will tend to fill up and once filled up, the irreversible traps will not influence trapping behaviors. Their model does not allow for the separate determination of capture and release rates for irreversible and reversible traps as long as both types of traps are simultaneously active. The analysis is limited for cases in which traps are nonsaturable and increasing in density. For example, during high hydrogen charging conditions, blisters can form in the material increasing trap density and altering trapping reactions. Also trap sites may be able to hold more

than one hydrogen atom at a time in contradiction to their model. Trap sites at sulfide-matrix interfaces are expected to be capable of holding hydrogen as pressurized gas instead of a single atom (23). Iino (23) has recently proposed a more generalized analysis of hydrogen trapping which deals with expressions for independent capture and release rates for irreversible and reversible traps. He also discusses several situations where low coverage irreversible traps are very active during diffusion processes.

Oriani (15) has given a thermodynamic interpretation to the McNabb-Foster theory which is based on the assumption that hydrogen at the lattice diffusion sites and hydrogen captured in traps are in local thermodynamic equilibrium, not only in the static situation but also during diffusion. The equilibrium assumption is expressed as

$$K = \frac{a_t}{a_L} = \exp\left(\frac{-\Delta E_x}{RT}\right) \qquad (10)$$

where

K = equilibrium constant

a_T = activity of hydrogen at a trap

a_L = activity of hydrogen at a lattice site

E_x = binding energy of the trap

R = universal gas constant

T = temperature, ^{o}K

Oriani's model (Figure 2) assumed that lattice-dissolved hydrogen, upon diffusing to within a small distance from an empty trap, could be captured. Each trap site can hold only one hydrogen atom. The trapping site represents an energy level lower than that of a normal site by E_x,

and it is bounded by an energy barrier of height $E^1 + E_a$, where E_a is the activation energy for jumping between normal lattice sites separated by the distance. The domain of validity of the assumption of local equilibrium is very broad. Low hydrogen coverage of traps and lattice site is assumed and the theory is founded on the postulate that the exchange of hydrogen between lattice and trap site occurs very rapidly.

Oriani has described several equations for effective diffusivity which are given by

$$D_{eff} = D_L (1 + KN_x/N_L)^{-1} \tag{11}$$

$$D_{eff} = D_L (1 + 3N_x/C_L^{o})-1 \tag{12}$$

where

D_{eff} = effective or experimental diffusivity

D_L = lattice diffusivity

K = equilibrium constant

N_x = number of trap sites per volume

N_L = number of hydrogen diffusion sites per volume

C_L^{o} = lattice concentration at the input surface

Equation 11 is based on the assumption that the fraction of occupied lattice diffusion sites and trap sites are sparingly occupied, and D_{eff} does not depend on lattice concentration. Equation 12 is based on the assumption that the traps are heavily occupied and a near saturation of the trap has occurred.

An important consequence of the local equilibrium hypothesis can be shown if Equations 9 and 11 are equated. The resulting relationship is given by

$$k/p = K/N_L \tag{13}$$

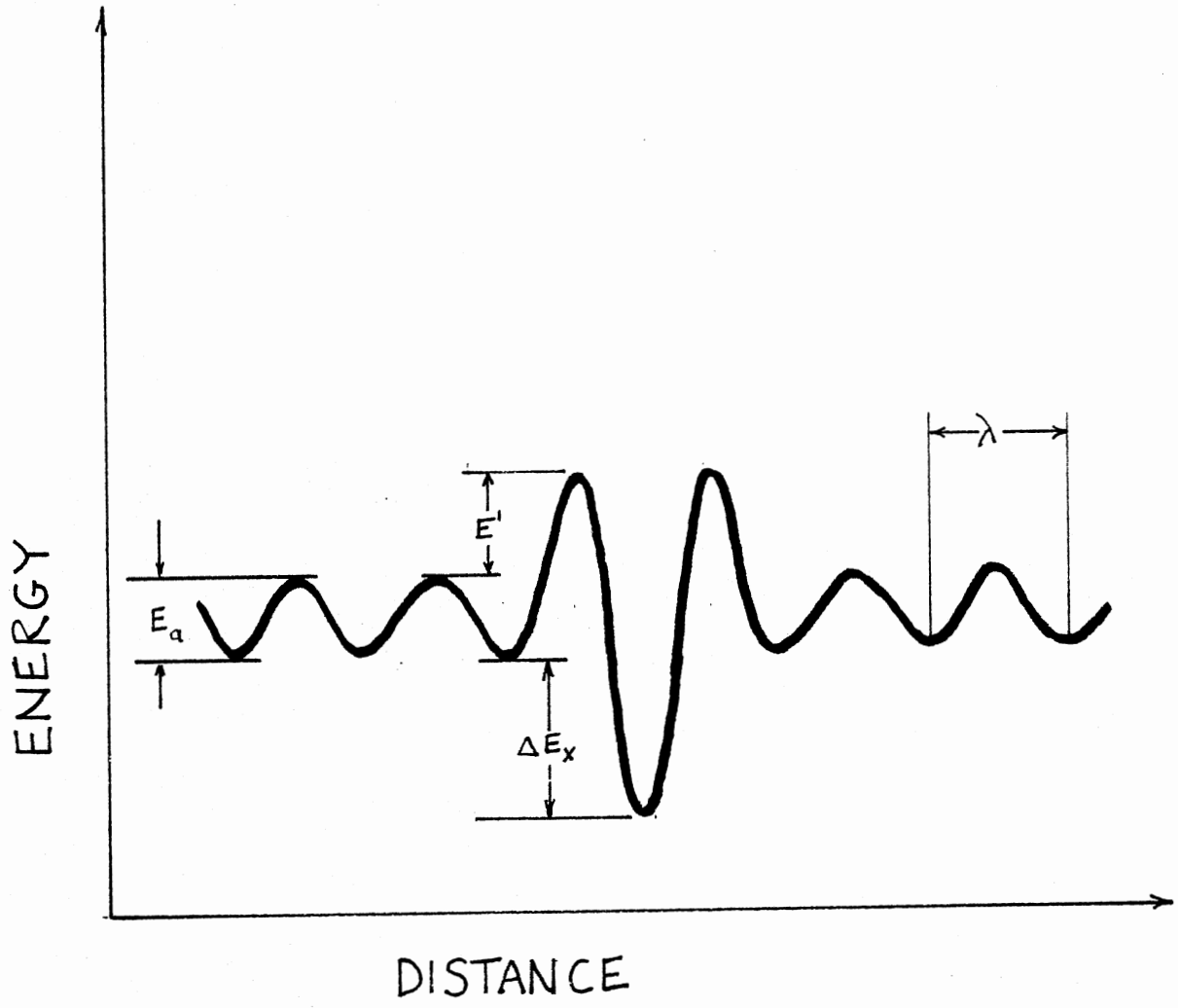

Figure 2. Oriani's Trapping Model

Equations 10 and 13 have been used by many authors in their analysis of hydrogen trapping to evaluate the parameters of Mcnabb and Foster's equations and to determine the trap binding energies of various types of traps.

A model which has recently been proposed considers the effect of hydrogen trapping on the embrittlement of steels. The model, developed by Pressouyre (16), is called the trap theory of hydrogen embrittlement (TTHE). Central to his theory, Pressourye follows a basic hypothesis that for hydrogen to embrittle a metal, it must exist at specific internal sites in a sufficient enough concentration to initiate the fracture process. The critical concentration depends on many factors related to the trap itself such as its shape, its location in the lattice, the state of stress at the site, etc. The TTHE also considers various situations where the following three groups of parameters are important:

1. the means by which hydrogen diffuses into the material (as dislocation atmospheres, or by interstitial diffusion, or along high diffusivity paths);
2. the location of hydrogen prior to the test (internal hydrogen versus external hydrogen); and,
3. the character of traps (irreversible versus reversible traps).

The extent of embrittlement is attributed in part to the means by which hydrogen moves in the material. Pressourye, in his model, suggests how dislocations can carry hydrogen atmospheres through the lattice, transferring hydrogen to structural defects or to other traps in the material. For instance, when a moving dislocation encounters a trapping site with a higher binding energy for hydrogen than does the dislocation, it will exchange hydrogen with this site. In this way, dislocations can pick up

or exchange hydrogen with stronger or weaker traps in order to satisfy equilibrium conditions. Dislocations and other traps are suggested to have both beneficial and detrimental contributions to the hydrogen embrittlement process. Pressouyre (16) suggests that a microstructure which would give optimal resistance to hydrogen embrittlement would contain a homogeneous distribution of small irreversible traps. The irreversible traps should not be potential flaws themselves and hydrogen must be effectively distributed among these traps. To test the model, Pressourye and Bernstein (24) have shown that a fine distribution of titanium carbide particles does indeed decrease susceptibility to internal hydrogen embrittlement. The TTHE appears to be useful as a general guide in selection of materials for use in hydrogen environments. However, the parameters involved in the model such as trap-hydrogen binding energy, trap shape and distribution, etc., need further characterization for commercial steels before the model can be employed effectively to determine hydrogen embrittlement for these metals under typical environmental conditions.

C. Transient Analysis

Numerical solutions to the McNabb-Foster equations, based on a finite difference method, have been developed by Caskey and Pillinger (17) (See Appendix B for a listing of the computer program that was developed in this study and based on the following approach). The McNabb- Foster equations are converted to dimensionless form as follows:

$$\frac{\partial u}{\partial \tau} + \frac{\partial w}{\partial \tau} = \nabla^2 u \tag{14}$$

$$\frac{\partial w}{\partial \tau} = \lambda u - \mu w - \nu uw \tag{15}$$

For the case of one dimensional diffusion, the variables can be defined as follows:

$$u = \text{relative concentration} = C/C_o$$

where C is the concentration of diffusant (number of species/cm^3 at X), and C_o is the surface concentration.

$$w = \text{relative trapped concentration} = nN/C_o$$

where N is the number of traps/cm^3, and n is the fraction occupied.

$$\tau = \text{reduced time} = Dt/a^2$$

where X is the distance from the specimen surface. the parameters λ, μ, ν describe the rate at which atoms are captured and released from the traps and are defined as:

$$\lambda = Nka^2/D \tag{16}$$

$$\mu = pa^2/D \tag{17}$$

$$\nu = C_o ka^2/D \tag{18}$$

where k is the rate of capture of diffusing atoms in a volume $kCN(1-n)\delta V$ and p is the rate of release in the volume $pnN\delta V$.

There are five parameters, C, D, k, p and N, in the McNabb-Foster analysis that must be known to solve the equations. The hydrogen concentration, C, at the input surface can be determined from steady state flux measurements. The lattice diffusivity, D, can be found from expressions such as those given by Equations 4, 5 and 6, and the other parameters can be found from careful evaluation of the numerical solution.

The computer analysis technique consists of fitting the curve of the theoretical model to the experimental permeation curve. The parameters λ, μ, and λ control the general nature of the diffusion equations, and these parameters are selected so as to provide the proper fit between the two curves. Once these parameters are known, it is possible to

determine other parameters such as k, p and N. Because there are many values of λ, μ, and ν that could provide a good fit of the experimental curves, no one set of parameters can be unique. However, if careful analysis is carried out, several relationships between different parameters can be established, thereby restricting the numerical values of the other parameters.

Pressouyre and Bernstein (24) have employed Oriani's reformulation of the McNabb and Foster diffusion model to analyze hydrogen trapping in several iron-titanium-carbon alloys. A permeation experiment similar to the one described in this study was employed to obtain hydrogen permeation transients. Irreversible trapping parameters were obtained from the first transients and reversible trapping parameters were obtained from the second transients since all irreversible traps were previously filled. Results of their study showed the following:

1. Titanium substitutional atoms are reversible, low occupancy traps with an interaction energy with hydrogen of 0.27 eV.

2. Titanium carbide particles are irreversible, high occupancy traps with an interaction energy with hydrogen of 0.98 eV.

Pressourye and Bernstein have demonstrated the attraction between titanium and hydrogen by the following theoretical evidence:

1. Titanium exhibits one of the most negative first order interaction coefficients in iron, and thus will be one of the most attractive elements for hydrogen. An upper limit to the thermodynamic driving force existing between elemental titanium dissolved in iron and hydrogen can be obtained by calculating the free energy of formation of the hydride TiH_2 in iron at room temperature.

2. Hydrogen dissolves in transition metals by ionizing; i.e., by

giving its electron to the collective election gas of the metal, thus existing as a screened proton. Since hydrogen introduces an excess electron, any impurity that introduces an electron vacancy will attract hydrogen to achieve local neutrality. Because titanium is on the left of iron in the periodic table, this suggests an attraction between titanium and hydrogen is of electronic origin.

In their analysis, Pressourye and Bernstein predicted titanium solute atoms were the major internal, reversible traps and that the hydrogen trap sites were any of the six octahedral sites nearest to a titanium atom. Since the composition of titanium in the alloys was known, the value of N_T (number of traps/cm^3), could be determined. Using Equation 9,

$$D_o/D = 1 + k/p\ N_T$$

the experimental value of D_o/D was plotted as a function of N_T and the slope, k/p, was found from the resulting linear relationship. They then determined the trap occupancy at steady state, n_s, by setting dn/dt = 0 and from Equation 8:

$$n_s = \frac{kC/p}{1 + kC/p}$$

The value of n_s was quite low, n_s = 0.0075, which reinforces their hypothesis that titanium is a low occupancy trap.

Pressourye and Bernstein next employed the numerical solution of Caskey and Pillinger (17) to find the unknown trapping parameters, k and p. From Equations 16, 17 and 18, the computer parameters are shown to be related to the experimental trapping values by the following:

$$\gamma/\mu = kN_t/p \tag{19}$$

$$\lambda/\nu = N_t/C \tag{20}$$

where all parameters have their previous meaning.

Since the approximate values of N_t, and C and the ratio k/p were known, the value of λ/μ and λ/ν could be found. Approximate values of λ and ν were then determined by fitting the theoretical permeation curve to the experimental curve, and from these values, the parameters k and p were determined. Further, the hydrogen trapping and release rates were found according to the following relationships:

$$\text{trapping rate} = kCN_T(1-n) \tag{21}$$

$$\text{release rate} = pN_T n \tag{22}$$

It was found, for one Fe-Ti-C alloy, that with a trapping rate of 5.9×10^{14} atoms H/s. cm^3 and $N_T = 1.48 \times 10^{20}$ atoms Ti/cm^3, that for any unit of time, only 4 Ti atoms/10^6 Ti atoms were actively participating in the trapping reaction.

Using Oriani's (15) assumption of dynamic equilibrium between diffusing and trapped hydrogen and from Equation 13, the equilibrium constant, K, was found as follows:

$$K = \frac{kN_o}{P}$$

where N_o is the number of octahedral diffusion sites in the ferritic bcc lattice = 2.5×10^{23} sites/cm^3.

Next, the interaction energy between titanium and hydrogen, E(Ti-H), was found. Equation 23, given by Oriani (15), and illustrated in Figure 1, is as follows:

$$E(Ti-H) = E^1 + E_a + E_x \tag{23}$$

where

E_x = trap site energy level that is lower than a normal site, but which is itself bounded by an energy barrier $E^1 + E_a$

E_a = 0.08eV, the normal diffusion activation energy in iron

E^1 = an additional step energy, which is of negligible importance.

From Equation 10, $K = \exp(-\Delta E_x/RT)$, and Equation 23, the interaction energy E(Ti - H) was found to be:

$$0.22 \text{ eV} < E(Ti - H) < 0.27 \text{ eV} \quad (24)$$

The titanium atom was thus found to have a trapping strength similar to dislocations and grain boundaries.

In the Pressourye and Bernstein analysis (24) above, several questionable assumptions and conditions are evident as outlined below:

1. The value of lattice diffusivity of hydrogen in iron ($D = 6.1 \times 10^{-6}$ cm^2/s) that they used is at least a factor of ten lower than most accepted values (15), (19).
2. The trapping rate was calculated in their analysis but not the release rate. It is found from their trapping values that the release rate is higher than the trapping rate at steady state. This implies that trapping is not taking place in the diffusion process, contrary to their basic assumption.
3. They also assumed the local equilibrium condition (15) between trapped and diffusing hydrogen. For this assumption to hold, the following conditions (25) must be met:

$$\mu \gg 1 \quad \text{and} \quad \nu \gg 1 \quad (25)$$

However, in their analysis, the computer parameter $\nu < 1$, invalidates their analysis.

D. Experimental Evidence of Hydrogen Trapping

Since its existence was first implied, hydrogen trapping has been well substantiated. Lacombe et al., (25) used an extremely sensitive technique, viz., high resolution autoradiography on tritium charged specimens, to study trap sites where hydrogen was found to concentrate. The material tested was a Fe-0.15 % Ti alloy (C= 15 ppm, N = 4 ppm and O = 40 ppm). The material was tested in several heat treated conditions so as to vary the distribution of precipitates and metalloid solute atoms (C, N and O) and to observe the variation of hydrogen trapping accordingly. Their observations suggest that the precipitate-matrix interfaces were the strongest traps in the material with a binding energy of 60.5 KJ/mole. The spherical precipitates, considered to be titanium carbide or carbo-nitride, were considerably stronger traps than the needle and plate like precipitates, which were determined by electron diffraction to be Fe_3N and TiN precipitates. The authors suggest that differences in trapping of the precipitates are due not only to chemical composition of the precipitates, but also to their size and shape. Pressourye (16) has noted the effect of trap size and shape on hydrogen trapping and has incorporated these parameters into his trap theory of hydrogen embrittlement. Other hydrogen traps found by Lacombe et al., were those at grain boundaries and at dislocations. The trap binding energies for these traps, 25-41 KJ/mole, are similar to those found by other authors (27), (28) who used different experimental techniques to analyze trapping. Bernstein (27) found a dislocation-hydrogen binding energy of 30.1 KJ/mole through the evaluation of tensile tests on hydrogen charged iron. In his experimental analysis, the Petch-Hall relation was used to

evaluate the contribution of effective stress acting on mobile dislocations. Gibala (28) used Schoeck's model of dislocation dragging of solute atoms in an experimental test to find the binding energy between hydrogen and dislocations. He reported a binding energy of 27.2 KJ/mole, again, in agreement with other findings for hydrogen-dislocation binding energy. It is interesting to note, however, the large discrepancy between the binding energy for titanium carbide particle as reported by Lacombe et al., (26), 60.7 KJ/mole, to that reported by Pressourye and Bernstein for the same alloy, 105.4 KJ/mole. Again, these values are based on the analysis from two different experimental techniques. Lacombe's technique was mentioned earlier and Pressourye and Bernstein used electrochemical charging and McNabb-Foster transient analysis. The credibility of each of these values of TiC-H binding energy needs to be ascertained.

Kumnick and Johnson (20) have identified microvoids and dislocations in iron as strong hydrogen traps. Armco iron was charged with hydrogen and changes in permeability and diffusivity were measured for specimens with varied amounts of mechanical deformation. In their analysis, they found that the evolution transients displayed longer time constants than the absorption transients. This effect was attributed to the condition in which traps are heavily occupied in the material. These authors found the trap density of the iron by using Equation 12 as:

$$N_t = \frac{C_o}{3}\frac{(D_L - 1)}{D_{eff}} \qquad (12)$$

At a deformation level of 40 % cold work, Kumnick and Johnson reported a trap density of 2.7×10^{22} m^{-3}. Since the trap density is less than the number of planes intersecting the dislocations, it is unlikely that the

trapping sites are associated with the long range elastic stress fields associated with the dislocations. Microvoids were also considered as major active traps, but ruled out because the iron studied showed no significant change in density upon rolling to 75% reduction in thickness. Evans (30), however, found a void volume in excess of 0.118% for cold-reduced iron. A hydrogen trap density corresponding to one hydrogen site per ferrite lattice cell in a void volume of 0.118% would give a trap density of approximately 10^{25} m^{-3}, a significant amount. In their recent paper (31), Kumnick and Johnson have determined the binding energy for traps to be 59.8 $\pm$ 4.6 KJ/mole which is about twice the value reported by other studies (27), (28). This rather substantial binding energy excluded the possibility of trapping based on elastic interaction between hydrogen and dislocations. Heterogeneous sites along dislocation cores, presumably jogs or multiple jogs, or the point defect debris left behind by the jogs of dislocations moving during plastic deformation were mentioned as possible trap sites.

Xie and Hirth (32) have presented data which shows the effect of carbon content and microstructure in steels on hydrogen permeability and diffusivity. Increasing carbon content in steel causes a decrease in diffusion path crossection and is reported to decrease the effective diffusivity of hydrogen in steel. Oriani (15) discussed the findings that trap densities tend to increase when carbon content or strength level of a steel are increased. When trap densities increase in a steel, the diffusivity of hydrogen in the steel decreases. Traps in steels occur at fine carbide particles in tempered martensite, at iron carbide particles in spheroidized steel and at interfacile areas between ferrite and cementite in the pearlite (33). Xie and Hirth (32) have shown normalized

1090 steel to have a lower diffusivity and permeability than spheroidized and quenched-tempered 1090 steel. An increased tortuosity of diffusion path for the pearlite structure of the normalized steels is mentioned as explaining these findings. Robertson and Thompson (33) found similar results for 1045 steel. However, they found that normalized 1045 steel has a lower trapping energy, 18.4 KJ/mole, than spheroidized and tempered martensite. They also found normalized 1045 steel to have a trap density of about 2.0×10^{19} cm^{-3}, less than the trap density of tempered martensite, about 2.6×10^{19} cm^{3}. The findings of Robertson and Thompson (33) seem to contradict the findings of Xie and Hirth (32) because the former authors' data indicates that diffusivity of hydrogen in the pearlite structure is larger than the diffusivity of hydrogen in tempered martensite or spheroidized steel.

Xie and Hirth (32) have recently reported the effect of a hydrogen recombination poison, thiourea, on the critical charging current that causes internal damage to 1090 spheroidized steel. They found that above a critical hydrogen-charging current, irreversible damage to the steel would occur in the form of blisters. Voids were found to have formed at Mn S inclusions rather than at carbides or grain boundaries. This effect agreed with results from microscopy studies which showed that the cohesive forces of ferrite-carbide interfaces and grain boundaries are large in comparison to those of Mn S-ferrite interfaces (32).

Beck et al., (34) found that in single crystal and polycrystal Armco iron the sites for void nucleation were not at grain boundaries but that the point of crack nucleation started at an aggregate of dislocations. Beck concluded that these findings were consistent with the fact that no blister formation occurred in the case of iron whiskers hydrogen charged

at high currents.

Xie and Hirth's results (32) suggest that blisters form when the internal pressure in interfacial cracks is large enough to cause the voids to grow by plastic deformation. Also, in their studies, they showed that the critical hydrogen charging current density corresponded to a critical pressure of P = 272 MPa, a fraction 0.68 of the yield strength of spheroidized steel. Consistent with this view, plasticity theory predicts that a critical pressure of 2/3 of the yield strength is needed to enlarge a spherical void by plastic deformation (32).

Pressourye (13) has recently classified traps according to the energy mechanism in which a trap captures a hydrogen atom. He lists several types of forces that could act on a diffusing atom in a crystal lattice. These forces are due either to electrical fields, stress fields, temperature gradiants or to the nonideal part of a chemical potential gradient. Another type of trap occurs when a diffusing atom randomly falls into an imperfection in the crystal lattice where it is energetically more favorable to stay. Pressourye gives examples of this type of trap as high angle grain boundaries, incoherent particle-matrix interfaces and voids. Pressouyre has also classified traps according to their shape, diameter, reversible or irreversible nature, and activation energy. Table I shows this classification.

TABLE I

CLASSIFICATION OF HYDROGEN TRAPS IN STEELS ACCORDING TO SHAPE

Trap Class	Example of Such A Trap		Interaction Energy* eV	Character if known	Influence Diameter D_1
	Vacancy				
Ponctual		Ni	(0.08)	most probably reversible	A few interatomic spacings
	Mn	Mn	(0.09)		
	Cr	Cr	(0.10)		
	V	V	(0.16)		
		Ce	(0.16)		
		Nb	(0.16)		
	Ti	Ti	0.27	reversible	
	Sc	O	(0.71)		
	Ca	Ta	(0.98)	getting more irreversible	
	K	la	(0.98)		
		Nd	(1.34)		
	Elements at the left of iron	Elements with a negative e^iH (interaction coefficient)			
Linear	Dislocations		0.31 0.25 (average values)	Reversible Reversible	30A for an edge dislocation
	Intersection of three grain boundaries		-	depends on coherency	-
	Vacancy				
Planar or bi-dimensional	Interfaces particle-matrix Ex: TIC (incoherent) Ex: Fe_3C Ex: MnS		0.98 0.8-0.98	irreversible, gets more reversible as the particle is more coherent	diameter of the particle or a little more as coherency increases
	Grain boundaries		0.27 Average value 0.55-0.61 (high angle)	Reversible Reversible = irreversible	Same as dislocation
	Twins		-	Reversible	A few interatomic spacings
	Internal Surfaces (Voids)		-	-	-
	-		-	-	-
Volume	Voids		>0.22		
	Cracks				
	Particles		depends on exothermicity of the dissolution of H by the particle		Dimension of the defect

Values of interaction energies are either experimental, or calculated (when between parenthesis) at room temperature.

Source: G. M. Pressouyre, "A Classification of Hydrogen Traps in Steel," MET. TRANS. A, 10A(1979), 1572.

CHAPTER III

EXPERIMENTAL

A. Equipment and Experimental Techniques

1. Cell Description

All hydrogen permeation experiments were carried out using an electrochemical technique first introduced by Devanathan and Stachurski (35). This technique, used quite extensively to obtain very accurate data on diffusivity and solubility of hydrogen in iron and steels, is capable of detecting fluxes as low at 6×10^{10} atoms H/cm^2 sec.

The electrolytic hydrogen permeation cell shown in Figure 3 was designed and constructed for use in obtaining permeation data. The schematic in Figure 4 shows the electrical circuit in connection with the cell. The cell consisted of two pyrex glass flanges, coupled with the membrane, and connected together with a pinch clamp. A water tight seal was produced by using rubber o-rings in the grooved glass flanges. The exposed specimen area was 19.6 cm^2. A Luggin capillary was positioned near the surface of the membrane facing the anode compartment. Counter electrodes in the anode and cathode compartments of the cell consisted of 16 gauge platinum wire. During permeation measurements, commercially pure nitrogen gas was continually bubbled through the 0.1 N NaOH solutions in order to displace residual oxygen and to promote stirring of the solutions.

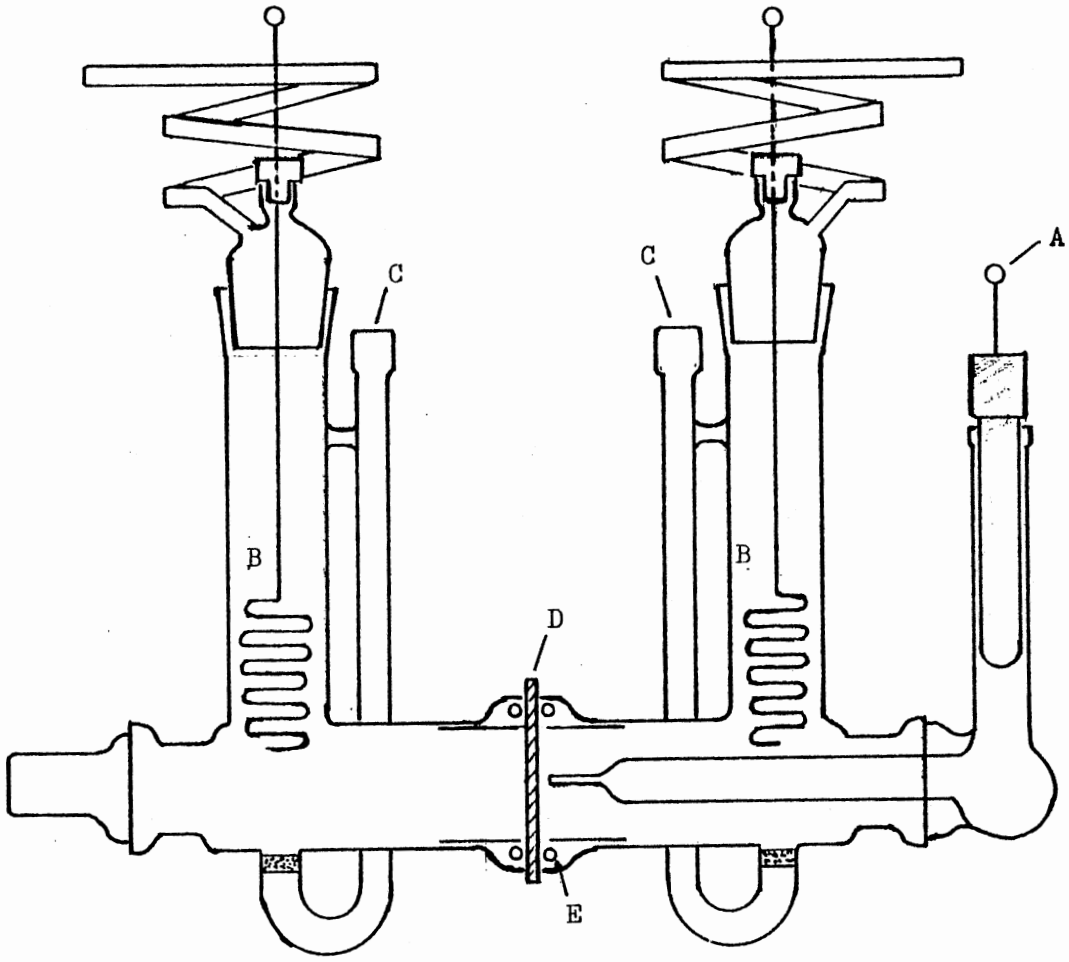

A. Luggin Probe/Reference Electrode
B. Platinum Counter Electrode
C. Nitrogen Gas Inlet/Outlet
D. Sample Membrane
E. o-Ring

Figure 3. Electrochemical Permeation Cell

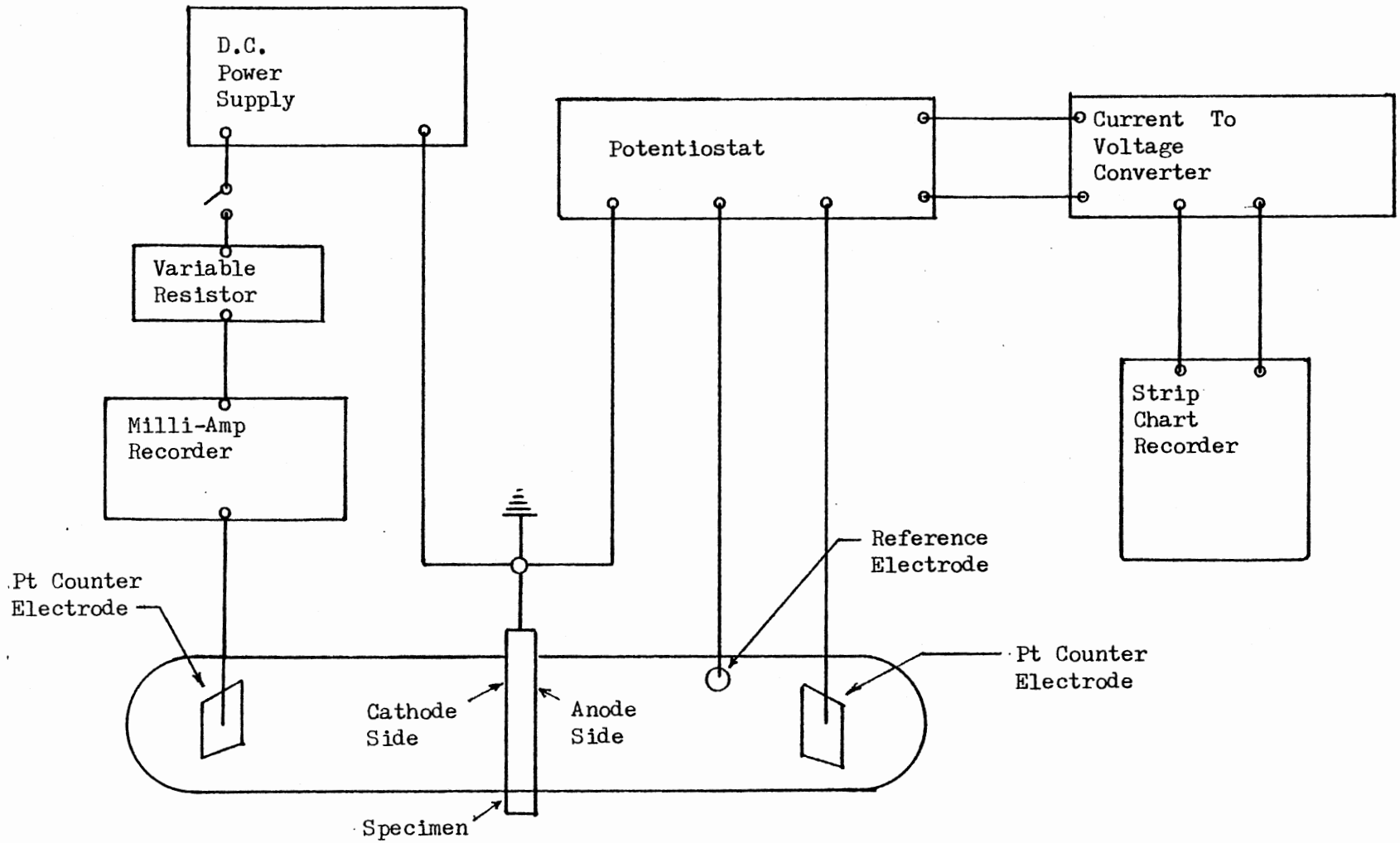

Figure 4. Schematic of the Electrical Circuit Connected to the Electrochemical Cell.

2. Cell Operation

The operation of the electrolytic hydrogen permeation cell consisted of maintaining a constant current density on the cathodic side of the membrane in order to introduce hydrogen charging. On the hydrogen exit or anodic side of the membrane, the amount of hydrogen that permeated through was measured as a function of time. The exiting hydrogen was measured electrochemically by maintaining the exit side of the membrane at a constant anodic potential of -300 mV versus a saturated Calomel reference electrode (SCE). Preliminary experiments suggested that at -300 mV (SCE), all the exiting hydrogen was oxidized. A Princeton Applied Research (Model 173) potentiostat applied the necessary current for hydrogen ionization while maintaining a constant potential. At this potential, the exiting H atoms were oxidized to H^+. Since this was the only electrochemical reaction at this surface, the current flowing in the anodic side of the cell was directly proportional to the number of H atoms permeating the membrane. Consequently, by recording the change in current with respect to time, the permeation transient could be measured.

In order to ensure that no unwanted reactions took place during the measurements, the electrochemical cell and glassware were meticulously cleaned. The following steps for preparing the cleaning solutions and palladium plating solution as well as other procedures in preparing the electrochemical cell are taken from Reference 36.

3. Cell Preparation

The following steps were taken in cleaning the glassware. It was immersed in a diluted soap solution and agitated for thirty minutes,

washed fifteen minutes in overflowing distilled water, boiled for thirty minutes in 1% H_2O_2 and rinsed for fifteen minutes in overflowing distilled water.

The platinum electrodes were electrochemically cleaned before use in a 5 v/o H_2So_4 solution. A current of 1.5 amps was passed for six minutes with the polarity changed at two minute intervals.

Solutions in both the anode and cathode compartments of the cell were in 0.1N NaOH made from reagent grade NaOH and distilled water. The solution was always deareated with nitrogen for twenty-four hours prior to use. It was necessary to displace oxygen from the solutions because any oxygen present would be electrochemically reduced and this would alter the permeation measurements. The use of NaOH ensures that no metal dissolution from the membrane will occur and thus the experimental conditions are better controlled than they would be if an acid electrolyte was used.

B. Sample Membranes

1. Material

The material chosen for this study was Armco iron and 1015 shim steel in sheet form. Chemical composition for the 1015 steel was not determined; however, this does not alter the purpose of this investigation as will be shown subsequently. The composition of the Armco iron is given in Table II. Samples of both materials were obtained in the cold rolled condition. Metallographic samples of the metals were prepared and microhardness measurements were made to check their metallurgical prehistory. The microstructure of the Armco iron showed ferrite grains that had been elongated by the rolling process. The 1015 steel had

an elongated ferritic grain structure, and a pearlite composition of about 15% and many inclusions which were probably sulfides, silicates and oxides. Microhardness measurements were Vickers 119 for the cold rolled Armco iron and Vickers 141 for the cold rolled 1015 steel. The tensile strength conversions for these microhardness measurements are 56 ksi and 67 ksi, respectively.

TABLE II

COMPOSITION OF ARMCO IRON USED IN THIS STUDY*

Element	Weight %
Aluminum	0.001
Carbon	0.002
Chromium	< 0.030
Copper	< 0.020
Manganese	0.001
Molybdenum	< 0.010
Nickel	0.080
Phosphorous	0.001
Silicon	0.005
Sulphur	0.003
Oxygen	0.009
Iron	Balance

*Analysis was supplied by Armco Incorporated, Middletown, Ohio.

Samples of the two materials were annealed in flowing Argon (commercial purity) for six hours at 800^{o}C. Except for a mild discoloration due

to limited oxidation which was subsequently removed by light polishing, essentially a bright anneal was obtained. Microstructural analysis of the annealed Armco iron showed an average grain size of about 80 microns, corresponding to ASTM grain size #4. The microhardness was Vickers 75. The grain size of the annealed 1015 steel was ASTM #5.5, and the microhardness was Vickers 85.

Armco iron was chosen in this research because of its high purity and low inclusion content. Carbide-particle traps are negligible in Armco iron although there are several other types of hydrogen traps that are present. If various trapping parameters can be characterized in iron, then these parameters could be used successfully as a basis to determine the hydrogen trapping behavior of say, 1015 steel. Two different heat treatment conditions for the material, cold roll and anneal, were employed to study the effect of increased trap density, and other trapping parameters, on the diffusion of hydrogen through the material. An explanation of hydrogen trapping effects relevant to this study and the parameters involved will be presented later.

2. Specimen Preparation

a. Polishing and Surface Cleaning. The as received material was cut into individual samples each 6 cm. (2.36 in.) by 6 cm. (2.36 in). The sample thickness was 0.025 cm. (0.01 in.) for the Armco iron and 0.023 cm. (0.009 in.) for the 1015 steel. The samples were then ground with silicon carbide grinding paper from 240 grit down to 600 grit. Next, the samples were successively polished with 5.0, 3.0, 1.0, and finally, 0.3 micron aluminum oxide abrasive polish. The shiny surface that resulted was found to be reproducible from sample to sample.

Before plating the metal surface with palladium, an extremely clean surface is necessary. Thus, a sequence of steps were carried out to clean the surface and remove the remnants of the passive or oxide film on the metal. First, the membrane was cathodically polarized for three minutes at a current density of 12 mA/cm^2 in a soap solution containing 53 g/l sodium dibasic phosphate (Na_2HPO_4) 15 g/l sodium hydroxide, 3 g/l sodium lauryl sulphate and 2 g/l ethylenediametetraecetic acid (EDTA). According to Reference 36, the above described cleaning procedure has the following effect:

> The very vigorous hydrogen bubbling, produced by the cathodic polarization, will tend to reduce any surface oxides. The chelating agent, EDTA, complexes with metals making their oxides fully soluble in alkaline solutions and thus prevents the redisposition of the oxides. Moreover, this procedure should lift off any soil adhering to the surface and the sodium hydroxide will convert any organic matter to soluble soaps (36, p. 12).

After the electrolytic cleaning procedure, the membrane was rinsed and ultrasonically agitated in a beaker of distilled water. The membrane was now ready for the plating operation.

b. Electroplated Palladium on Membrane Surfaces. The membrane surfaces were plated with a thin palladium coating to prevent anodic dissolution of the metal at the operating potential. Iron and steel can form passive or oxide films that result in hydrogen surface entry effects. The palladium coating gives an inert surface free of hydrogen blocking effects. The Pourbaix diagram or potential-pH diagram for palladium (37) indicates that palladium surfaces should be thermodynamically stable in the environmental conditions imposed during the permeation measurements.

The palladium plating set up consisted of connecting the membrane to be plated as the cathode and placing it between two platinum wire

anodes in a 1000 ml beaker that had been partially filled with deareated 0.1N solution. A saturated Calomel reference electrode was then positioned near the membrane surface. A glass tube extended into the solution so as to displace oxygen and to promote stirring of the solution during the plating operation.

Six ml of the plating solution was then added to the NaOH solution. The plating solution contained $Na_2Pd(NO_2)_4$ formed by dissolving lg palladium chloride ($PdCl_2$) in 100 ml of distilled water and reacting the palladium chloride with sodium nitrite ($NaNO_2$). Palladium was plated onto the metal surface by maintaining the surface at 1200 mV (SCE) for three hours.

From the total amount of Pd ions in solution, the palladium electrodeposits were estimated to be about 1 μm thick. Since the palladium thickness was so small compared to the membrane thickness and because hydrogen has a higher solubility for hydrogen than does iron and steel, the palladium does not measurably alter the transport of hydrogen.

The samples were microscopically examined both optically and by scanning electron microscopy to check for plating integrity and porosity. Some porosity of the palladium coating was found where the coating did not cover inclusions on the 1015 steel. For these samples, a slightly thicker palladium coating was applied in order to cover these pores. No such discrepancies were found in Armco iron samples.

CHAPTER IV

RESULTS AND DISCUSSION

A. Results

Typical data and reproducibility of results for cold worked iron are shown in the successive absorption transients in Figure 5. These transients are for the same Armco iron specimen at the highest current density used in the study. Successful obtainment of accurate permeation data depends, in part, on the following experimental conditions:

1. electrochemical cell cleanliness;
2. condition of the membrane (internal damage or external corrosion); and,
3. sensitivity of the instruments connected to the electrochemical-cell circuit.

The procedure used to clean the electrochemical cell was described in the Experimental section. This cleaning procedure was found to give very good results, again suggested by the reproducibility of transients. Impurities in the electrochemical cell solutions could cause unwanted reactions during the experiment and mask the permeation current.

Corrosion problems were encountered during the initial development of the experiment. Pitting of the membrane was discovered where the membrane touched the o-ring seal. This problem was eliminated by applying silicon grease to the seal. Another corrosion problem occurred as the

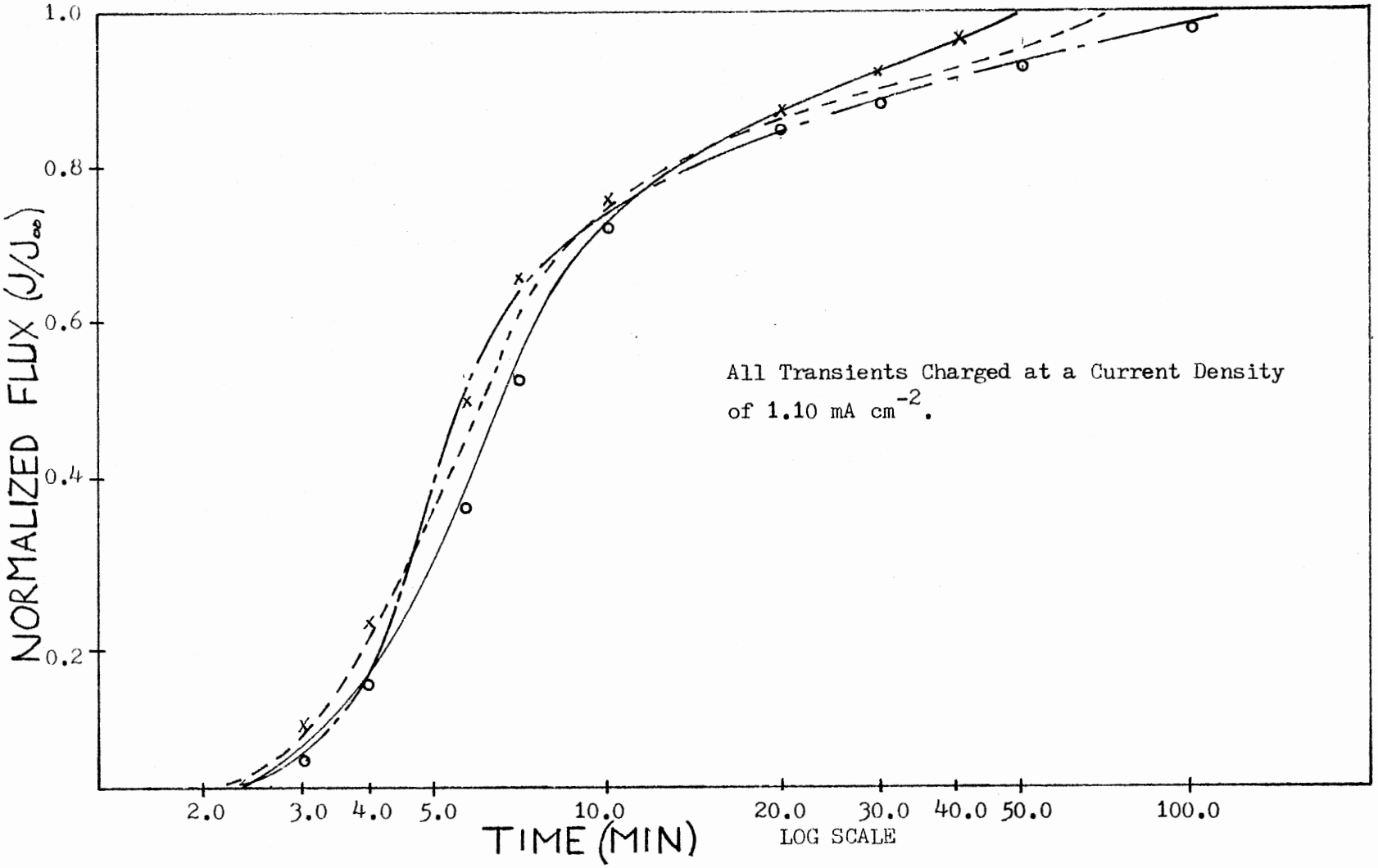

Figure 5. The Reproducibility of Absorption Transients for Iron.

result of a deficient palladium coating on the membrane. Pores in the palladium coating led to rapid localized corrosion of the membrane during trial permeation experiments. The porosity in the coating was due to an inadequate surface cleaning procedure. Several surface cleaning procedures were attempted, and it was found that the cleaning procedure given in the experimental section was usually adequate as long as the soap solution was thoroughly rinsed off the specimen. The specimens were ultrasonically agitated for a few minutes after the rinse, and then immediately put into the plating solution. Palladium plating solutions that had been stored over approximately a month were found to give unsatisfactory results.

The thickness of the palladium coating was estimated from knowing the weight of the palladium in the plating solution, the density of palladium and the surface area of the plated specimen. Another way of estimating plating thickness would be to use Faraday's law and the following relation:

$$m = \frac{It \times \text{Eq. wt.}}{F} \tag{26}$$

where

m = mass of the electrodeposit

I = plating current density

t = time or duration of plating process

Eq. wt. = Equivalent weight of deposited species

F = Faraday constant, 96,500 coul. (gm. eq.)

From the above equation, the mass of the palladium deposit can be determined. The thickness of the deposit is determined by dividing the mass by both the density of palladium and the surface area of the plated specimen. However, the former scheme gives an upper limit on the plating

thickness.

Normally, during operation of the electrochemical cell, the current is monitored between the counter electrode and the membrane or working electrode while a constant potential is imposed between the working electrode and the reference electrode. The current is measured by the potentiostat on a very sensitive microampere scale. Before the permeation experiment can be begun, it is necessary to reduce the current in the anodic chamber of the cell to a very low background current which lies in the 1μA range. The reduction of the background current is necessary so that only the change in current due to the oxidation of hydrogen is detected. One problem encountered during the initial development stage of the experiment was that of static interferences in the current signal of the potentiostatic circuit such that a low background current could not be achieved. Background current can be affected by stray currents from the room lights, operating machinery, static discharges, or even from cosmic radiation. These problems were eliminated by shortening the cable to the reference electrode after it was found the cable was acting as an antenna and was picking up stray signals. A better ground line to the potentiostat was also installed, and after making these changes, background currents of 0.1μA could be obtained.

Effective operation of the electrochemical cell, in part, depends on the premise that a constant current will provide a constant hydrogen fugacity on the input side of the membrane and that all the exiting hydrogen will be oxidized on the anodic side of the membrane. The current source used in this study provided a constant charging current that was easily adjustable from the voltage control knob on the D.C. power supply. Figure 3 shows the electrical circuit used in the experiment. The value

of the resistor in the circuit was chosen so that the desired degree of sensitivity in current control could be obtained.

Preliminary experiments were performed to find the optimum anodic potential where complete oxidation of hydrogen would occur and where anodic dissolution of the membrane would not occur. This experiment consisted of producing a potentiostatic polarization curve while a constant hydrogen flux permeated the membrane. This curve is shown in Figure 6. An anodic potential range of -300 to -100 mv (SCE) was found to be optimum. Since this was the highest value of permeation current in the study, it was ascertained that for this anodic potential range, all permeating hydrogen would be oxidized. A separate experiment was carried out to determine if anodic dissolution or corrosion of the membrane would occur while being held in the previously mentioned anodic potential range for an extended amount of time. A continually increasing steady state permeation current is attributed to corrosion of the membrane (38). During the experiment, a specimen was charged over night (12 hours) so that any changes in steady state flux could be detected. It was found that at the end of the experiment the permeation current had changed by 8% from the first three hours. This is a relatively slight change in current and is thought to be due to an increase in trap density or to drift in the charging current. A microscopic examination of the specimen did not reveal any corrosion.

Several permeation experiments were carried out using a hydrogen charging solution that contained arsenic, a hydrogen recombination poison. Figure 7 shows the absorption transients of 1015 steel charged with the arsenic solution. Table III shows the effect arsenic has on hydrogen diffusion and permeation parameters. At a constant charging current,

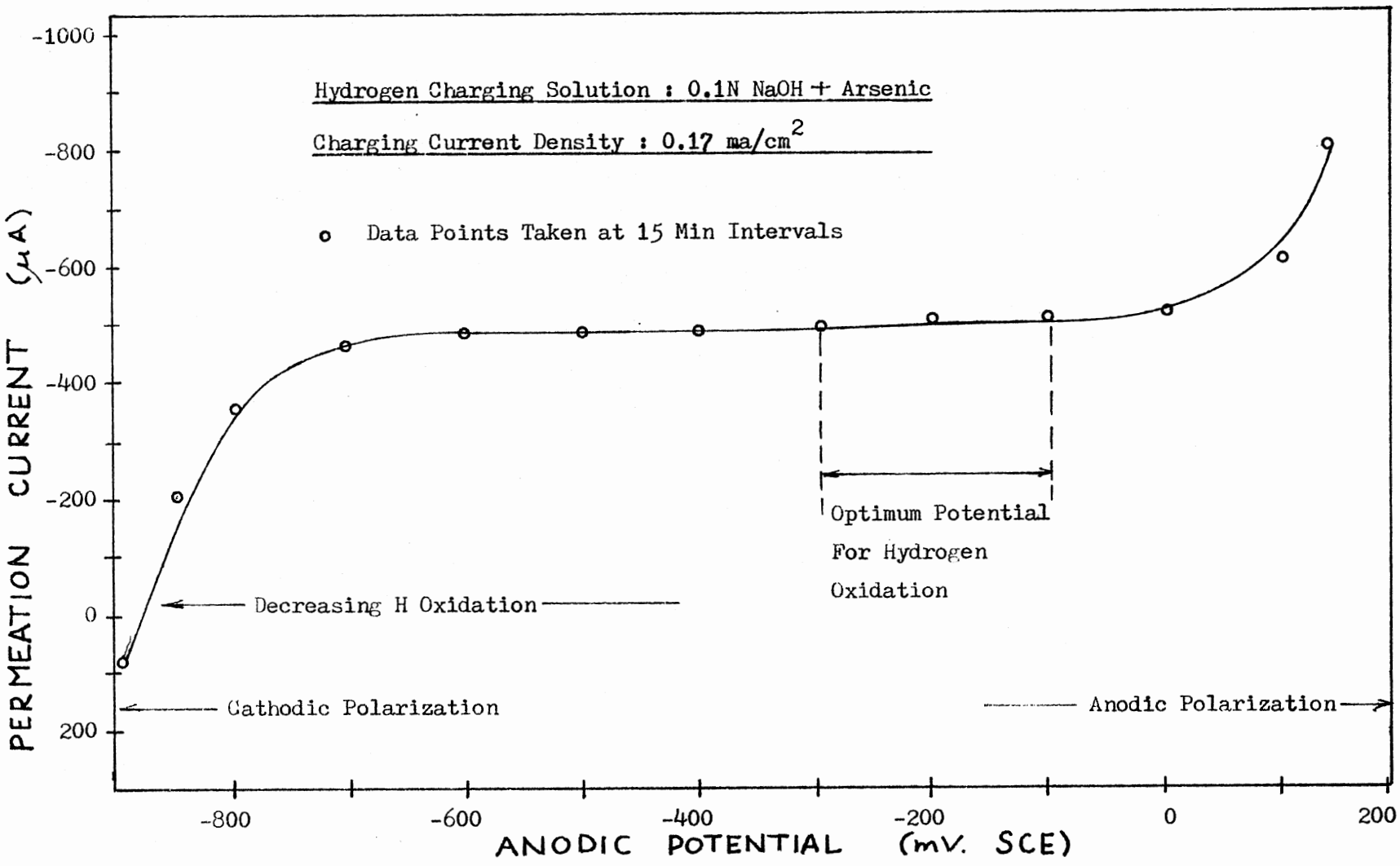

Figure 6. Permeation Current Versus Hydrogen-Oxidizing Potential.

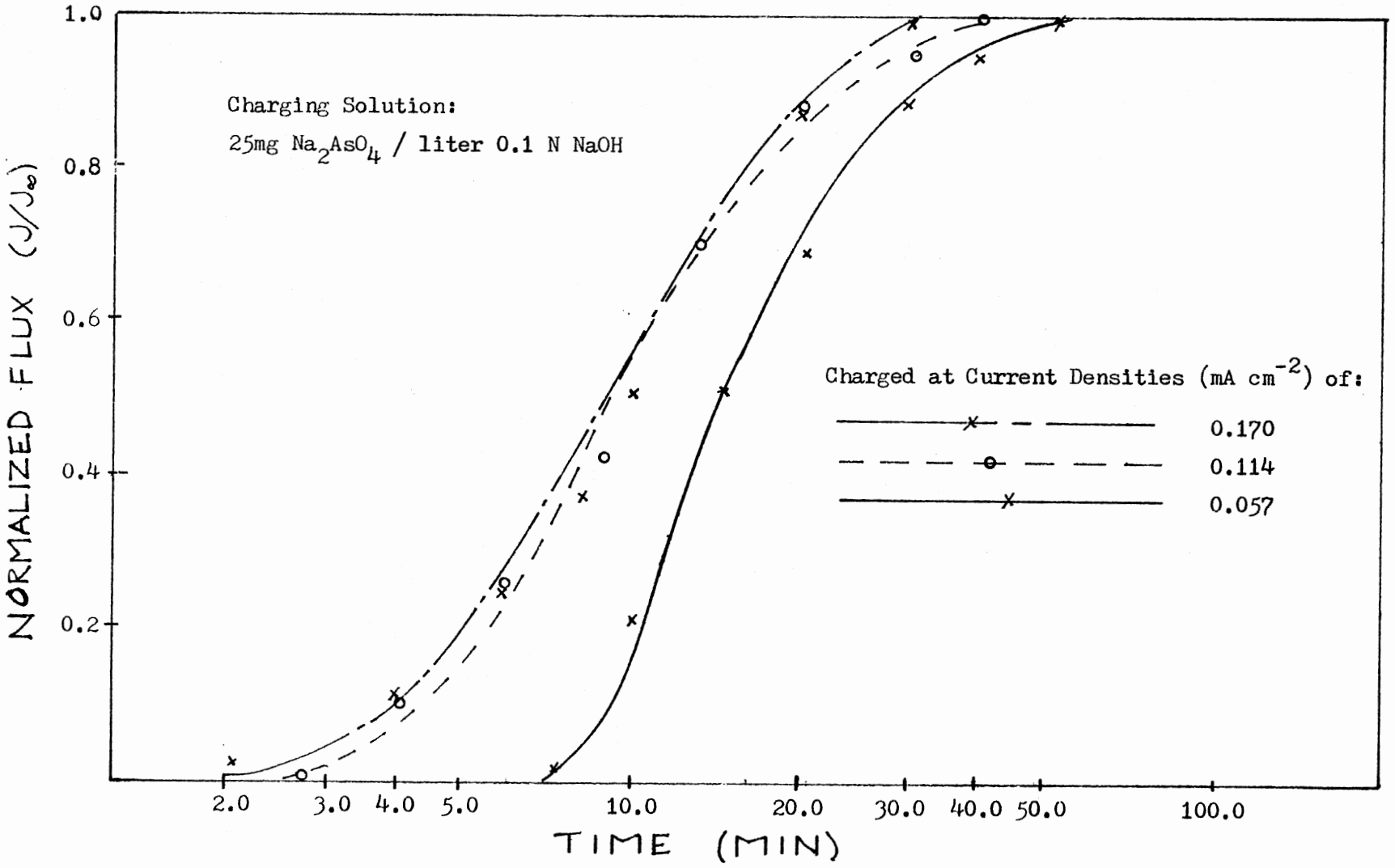

Figure 7. Rise Transients for Cold-Worked 1015 Steel in an Arsenic Charging Solution.

TABLE III

FIRST AND SECOND RISE AND DELAY TRANSIENTS
FOR ARMCO IRON AND 1015 STEEL

Speciman and Charging Current, I_c (mA/cm)	Effective Diffusivity, D_{eff} (cm^2/sec)			
	First Rise Transient	Second Rise Transient	First Decay Transient	Second Decay Transient
Cold Worked Armco Iron L = 0.02 cm I_c = 0.62	1.82×10^{-8}	1.39×10^{-7}	7.81×10^{-8}	2.01×10^{-7}
Cold Worked 1015 Steel L = 0.023 cm I_c = 0.62	9.80×10^{-9}	1.41×10^{-7}	1.41×10^{-7}	1.47×10^{-7}
Cold Worked Armco Iron(1) L = 0.02 cm I_c = 0.057	2.37×10^{-8}	8.2×10^{-8}	8.33×10^{-8}	8.33×10^{-8}
Cold Worked 1015 Steel(1) L = 0.025 cm I_c = 0.17	4.27×10^{-8}	1.8×10^{-7}	4.48×10^{-7}	4.5×10^{-7}

(1) Charging solution contained Na_2AsO_4.

steady state flux is increased by approximately a factor of ten over the flux of a solution that does not contain arsenic. This result in itself is significant because it has the effect hydrogen recombination poisons have on hydrogen entry processes. Increased hydrogen entry into a steel would increase the steel's susceptibility to hydrogen embrittlement. It was also interesting to find that there was a linear relationship between steady state permeation current and charging current density as shown in Figure 8. Another author (39) has also reported this effect for arsenic charging solution. Figure 9 shows the permeation current versus charging current for cold worked 1015 steel in 0.1 N NaOH without arsenic additions. The permeation current is shown to vary approximately as the square root of the charging current and this relationship is similar to the one given by Bockris (40). The results of Figures 8 and 9 are presented together on Figure 10 to show the drastic effect arsenic has on hydrogen absorption and coverage kinetics. Arsenic increases the hydrogen coverage on the membrane surface, and this gives a permeation current that varies directly as the charging current.

The Armco iron and 1015 steel used in this study were annealed in flowing argon (96%) at 800^{o}C for 6 hours. Previously, there was an attempt to anneal other specimens in nitrogen (99.6%) in a ceramic container that was placed in an oven. The ceramic container was closed except for a small opening through which a stainless steel tube carrying the nitrogen gas was placed. After 6 hours of annealing at 800^{o}C, the oven was turned off, and after it cooled down, the specimen was taken out and examined. A thick, black scale had formed on the specimens making them unacceptable for use as specimens in the permeation experiment. This method of heat treating was discontinued, and the argon gas annealing

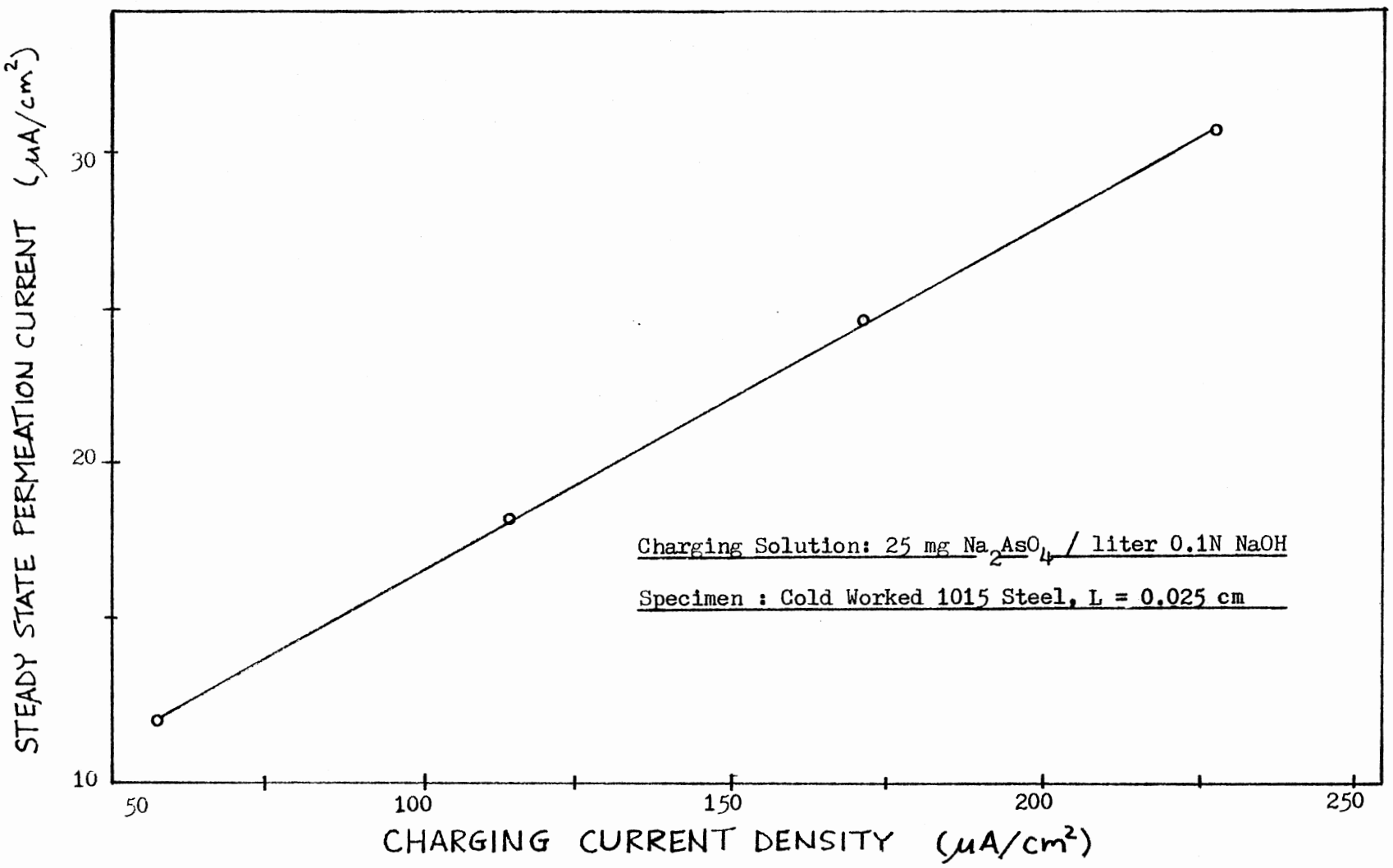

Figure 8. Permeation Current Versus Charging current for 1015 Steel in an Arsenic Charging Solution.

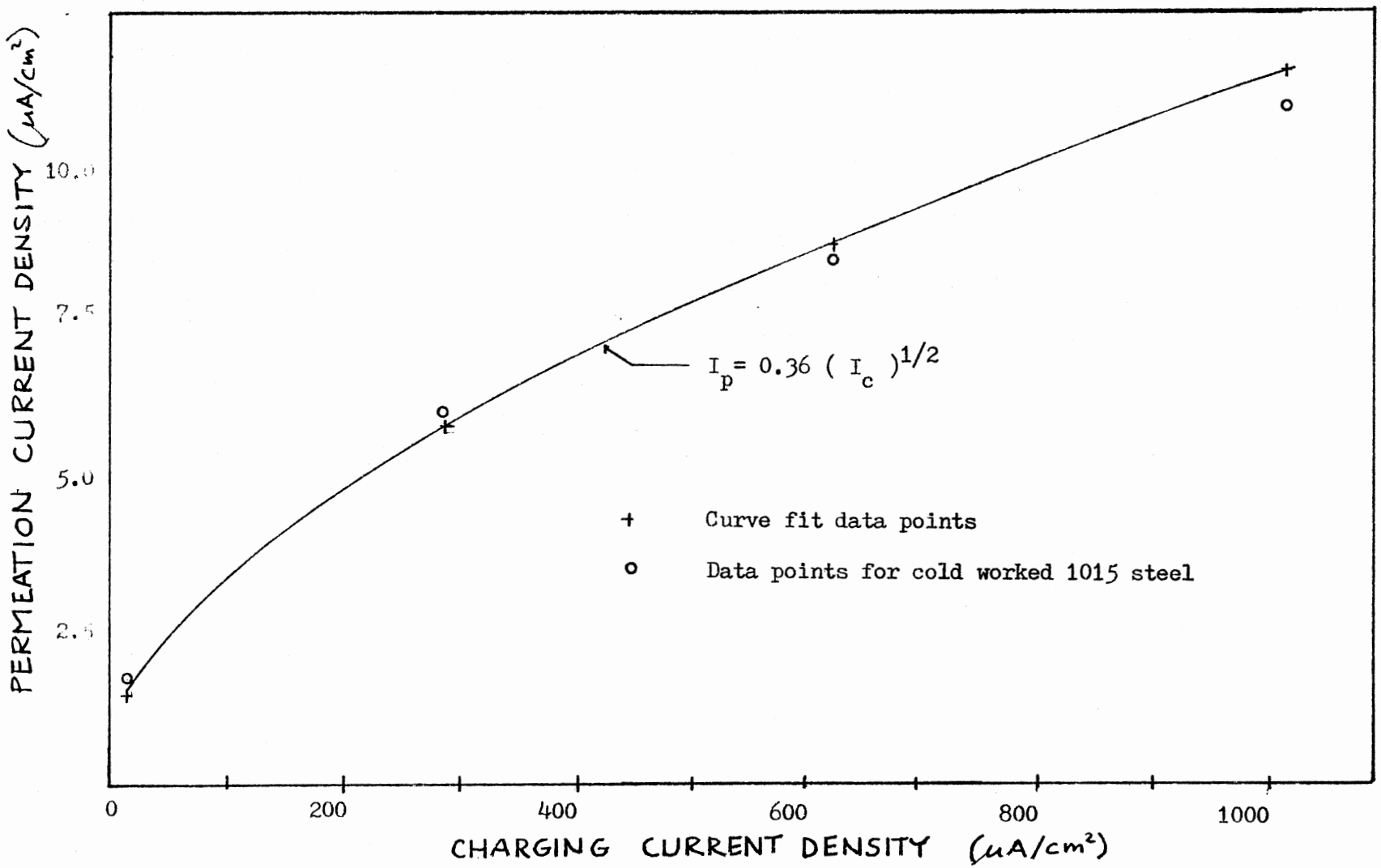

Figure 9. Permeation Current Versus Charging Current for 1015 Steel in a 0.1N NaOh Charging Solution.

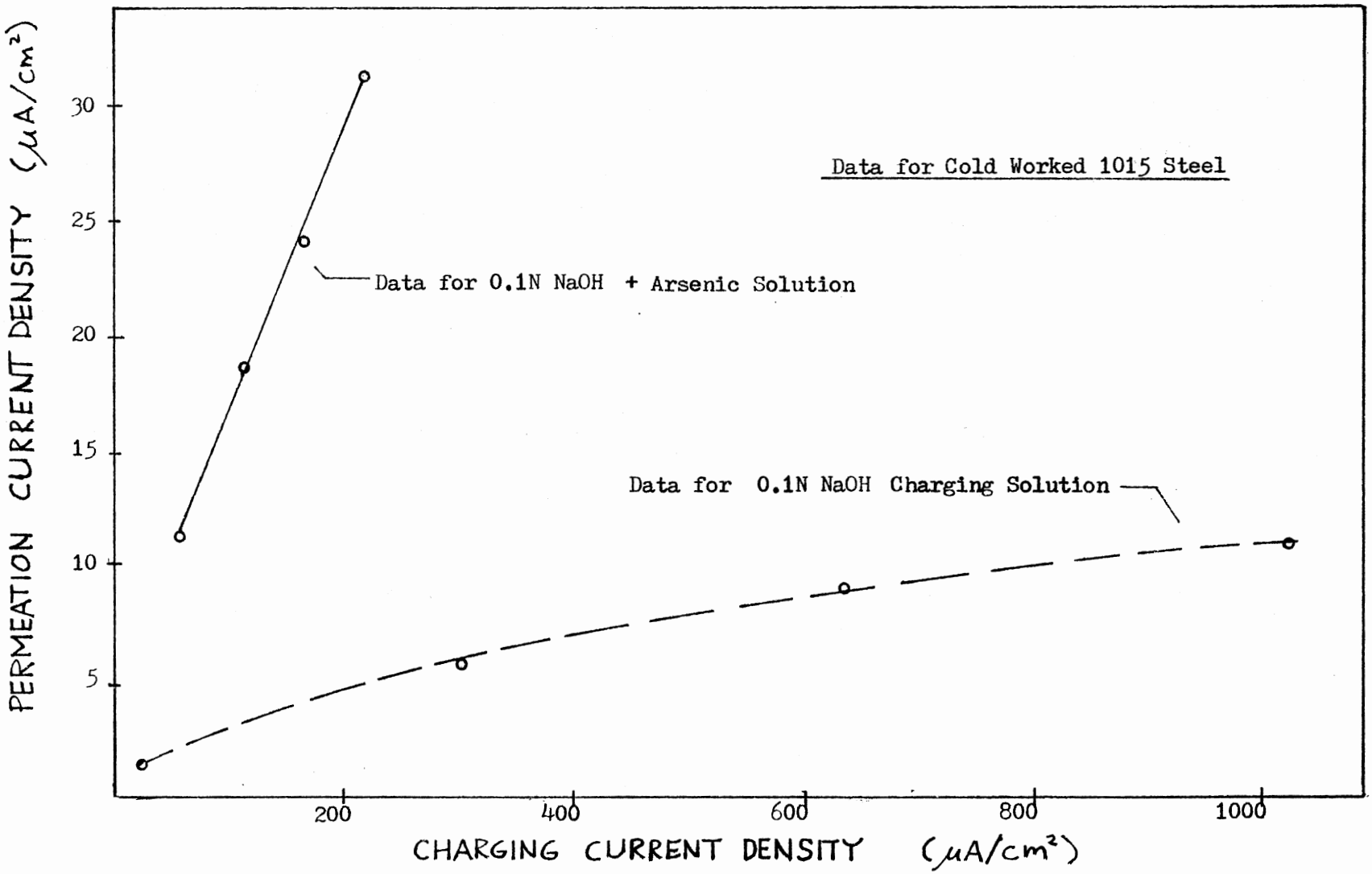

Figure 10. Comparison of Permeation Behavior in an Arsenic Charging Solution and in a 0.1N NaOH Charging Solution.

method, described earlier, was ensued.

Figure 11 shows the result of the first permeation transients for cold worked iron and 1015 steel. The 1015 steel transient is shown to increase more rapidly during the initial part of the permeation then drop below the rise transient of the iron. The 1015 steel takes longer to reach steady state than the iron and has a lower diffusivity than that of the iron. Table IV gives the values of diffusivity for the specimens. The diffusivity of 1015 steel is lower than that of the iron by approximately a factor of 10. Table IV also shows an increase in diffusivity of the second transients for the Armco iron and 1015 steel. The difference in the diffusivities between the first and second transients indicates the degree of irreversible trapping that is taking place in the material. During the first transient, both reversible and irreversible trapping reactions are taking place. However, during the second transient, only reversible trapping is taking place because all irreversible traps were previously filled. Irreversible traps have high hydrogen-binding energies, above 75 KJ/mole (13). Consequently, these traps hold hydrogen very tightly such that once the traps are filled, they are removed from the trapping process (under the conditions of the present study; i.e., temperature, time, etc.). Irreversible traps in Armco iron might be inclusions, grain boundary-particle interfaces and carbide particles. The Armco iron used in this study had a very low carbon content (0.002 wt. %); however, this is slightly greater than the solubility limit of carbon in iron at room temperature, and therefore, some iron carbide will be present in the iron. Manganese sulfides, oxides and inclusions probably make up the largest densities of irreversible traps. The much higher inclusion content and carbide particle content of the 1015

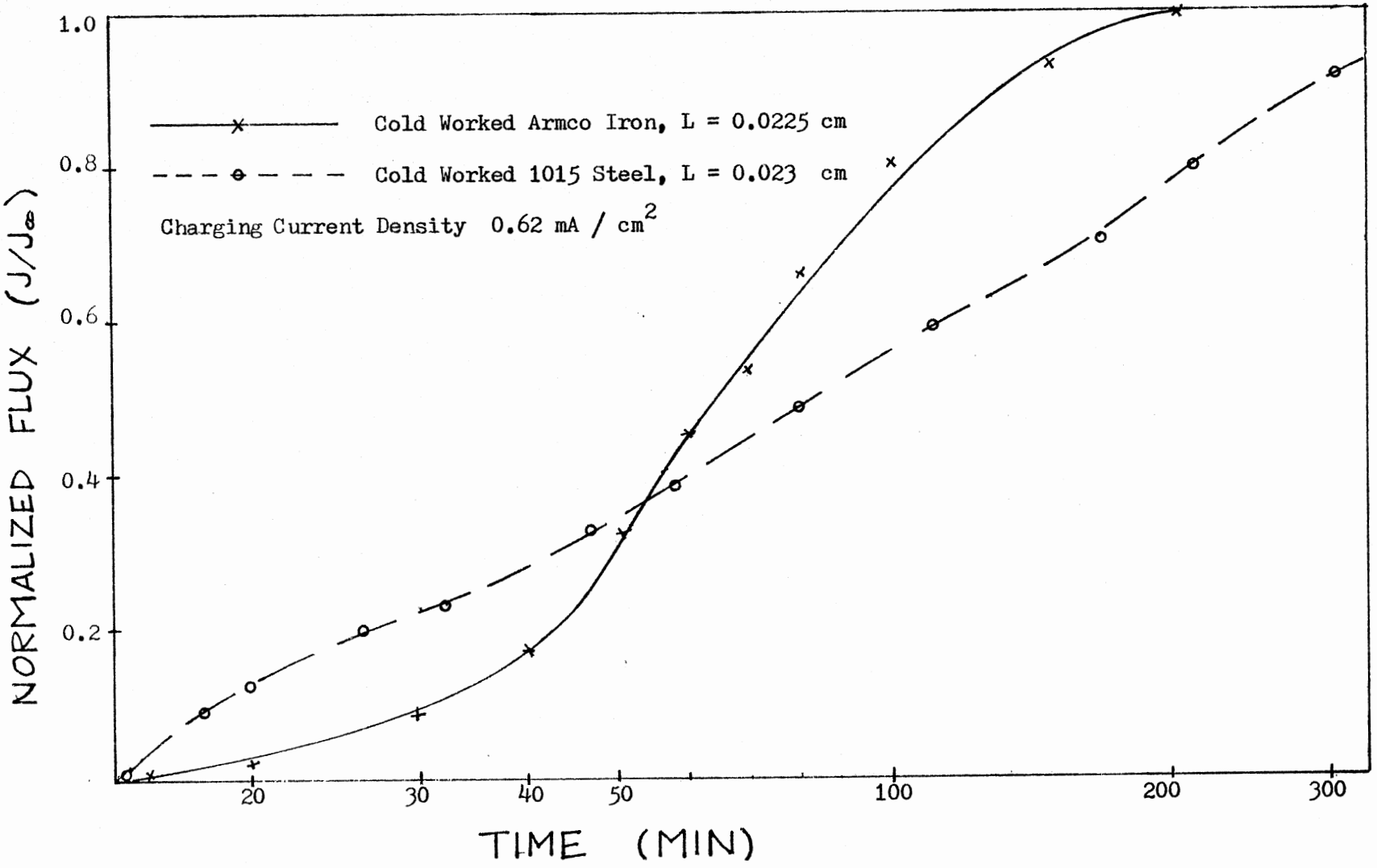

Figure 11. First Permeation Transients for Cold-Worked Armco Iron and 1015 Steel.

TABLE IV

COMPILED ABSORPTION AND EVOLUTION
DIFFUSIVITY VALUES

Specimen and Thickness cm	Charging Current Density ma/cm^2	Steady State Permeation Current Density ua/cm^2	Absorption D_{eff}(1) cm^2/sec ($\times 10^6$)	Absorption D_{eff}(2) cm^2/sec ($\times 10^6$)	Evolution D_{eff}(1) cm^2/sec ($\times 10^6$)
Annealed(3)	0.03	0.91	1.20	0.99	1.69
Armco Iron	0.28	2.60	3.20	2.78	4.32
	0.62	3.84	8.10	7.29	10.15
L = 0.018	1.10	5.40	9.70	9.10	10.20
Annealed(3)	0.03	1.11	0.77	0.54	1.86
1015 Steel	0.28	2.82	2.20	1.94	2.10
	0.62	4.10	4.90	4.20	7.10
L = 0.019	1.10	5.82	9.00	7.60	11.60
Cold Worked(3)	0.03	1.10	0.07	0.06	0.05
Armco Iron	0.28	3.21	0.11	0.11	0.15
	0.62	4.30	0.14	0.12	0.20
L = 0.020	1.10	6.60	0.17	0.17	0.20
Cold Worked(3)	0.03	1.71	0.03	0.02	0.09
1015 Steel	0.28	6.12	0.11	0.08	0.11
	0.62	8.67	0.15	0.14	0.15
L = 0.023	1.10	10.65	0.17	0.16	0.32
Cold Worked(4)	0.057	6.38	0.11	0.08	0.08
Armco Iron	0.080	8.21	0.25	0.25	0.16
L = 0.02					
Cold Worked(4)	0.057	11.79	0.10	0.10	.28
1015 Steel	0.114	18.20	0.18	0.16	.42
	0.170	24.59	0.18	0.16	.45
L = 0.025					

(1) Determined using Equation 35 for D_{eff}.

(2) Determined using Equation 36 for D_{eff}.

(3) Charging solution contained 0.1N NaOH.

(4) Charging solution contained 0.1N NaOH + Na_2AsO_4.

steel indicates the significant effect these irreversible traps have on delayed hydrogen diffusion during the first transient as shown by the low value of diffusivity in Table IV. These results indicate a much higher irreversible trap density in the 1015 steel as compared to the Armco iron.

Figures 12, 13, 14 and 15 show a series of second rise transients for Armco iron and 1015 steel in both the annealed and cold worked state. The effective diffusivities for these transients were calculated by two different methods. The first method was the Laplace technique (36) given by Equation 35, and the second method was the time lag method (35) given by Equation 38. Equations 34 and 37 and their descriptions are given in Appendix A. Table IV gives the values of hydrogen diffusivity in the materials at increased charging currents calculated by both methods. Each of the methods for calculating diffusivity gave similar results. Table V gives relevant permeation data for these transients such as hydrogen input concentrates and permeability.

Typically, a series of successive permeation experiments was done on one specimen at increased stepped charging currents. Since the first transient filled up irreversible traps, only reversible trapping was analyzed in the next transients. Figures 12, 13, 14 and 15 show that the transients are shifted to shorter times and reach steady state more rapidly as the charging current density increases. Namboodhiri and Nanis (41) also found this effect in Armco iron. They showed that hydrogen diffusivity in Armco iron is dependent on the hydrogen concentration within the metal. Figure 16 depicts a concentration dependent diffusivity for cold worked 1015 steel up to a particular limiting hydrogen input concentration where the diffusivity becomes constant. The present

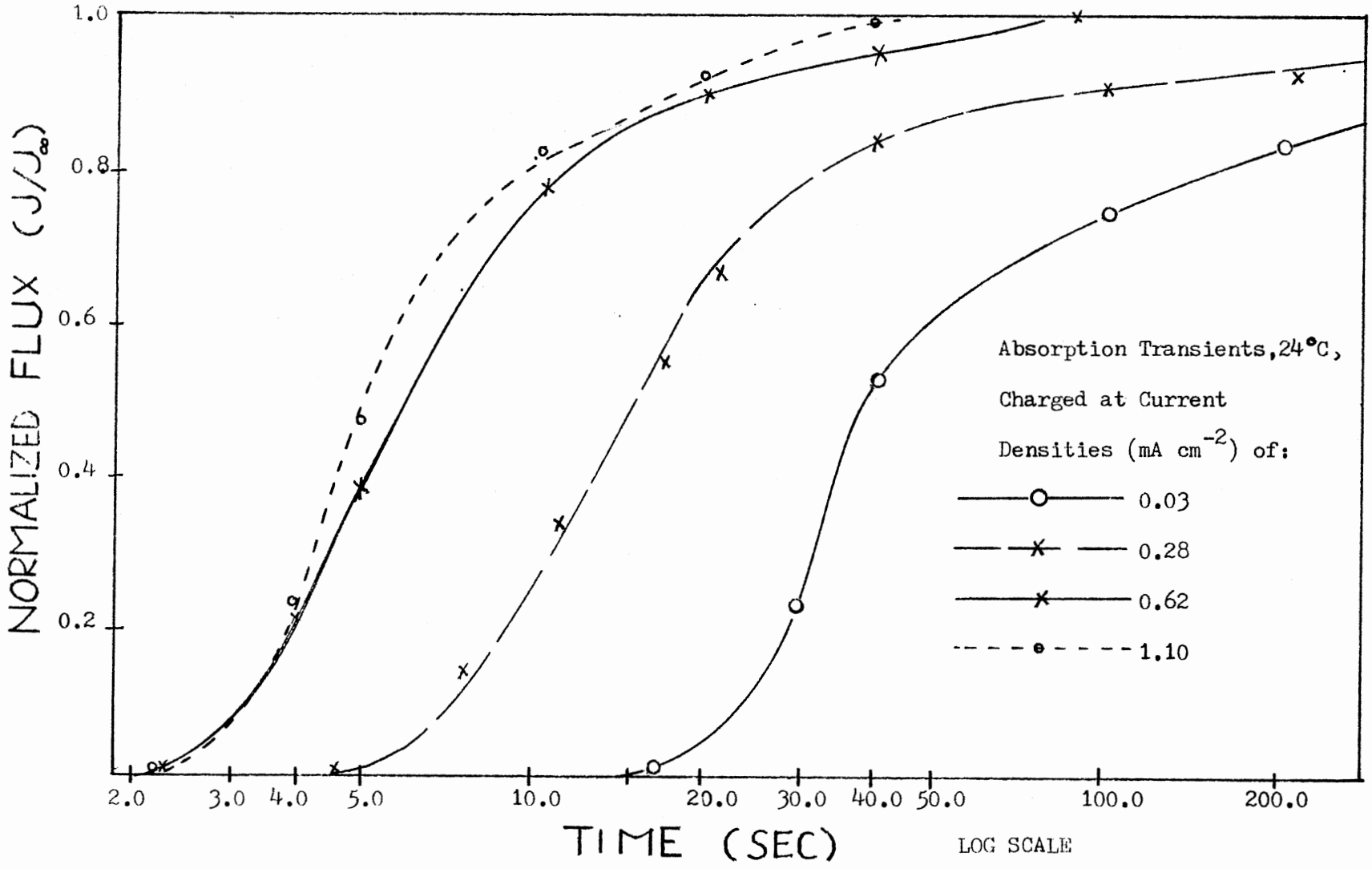

Figure 12. Rise Transients for Annealed Armco Iron.

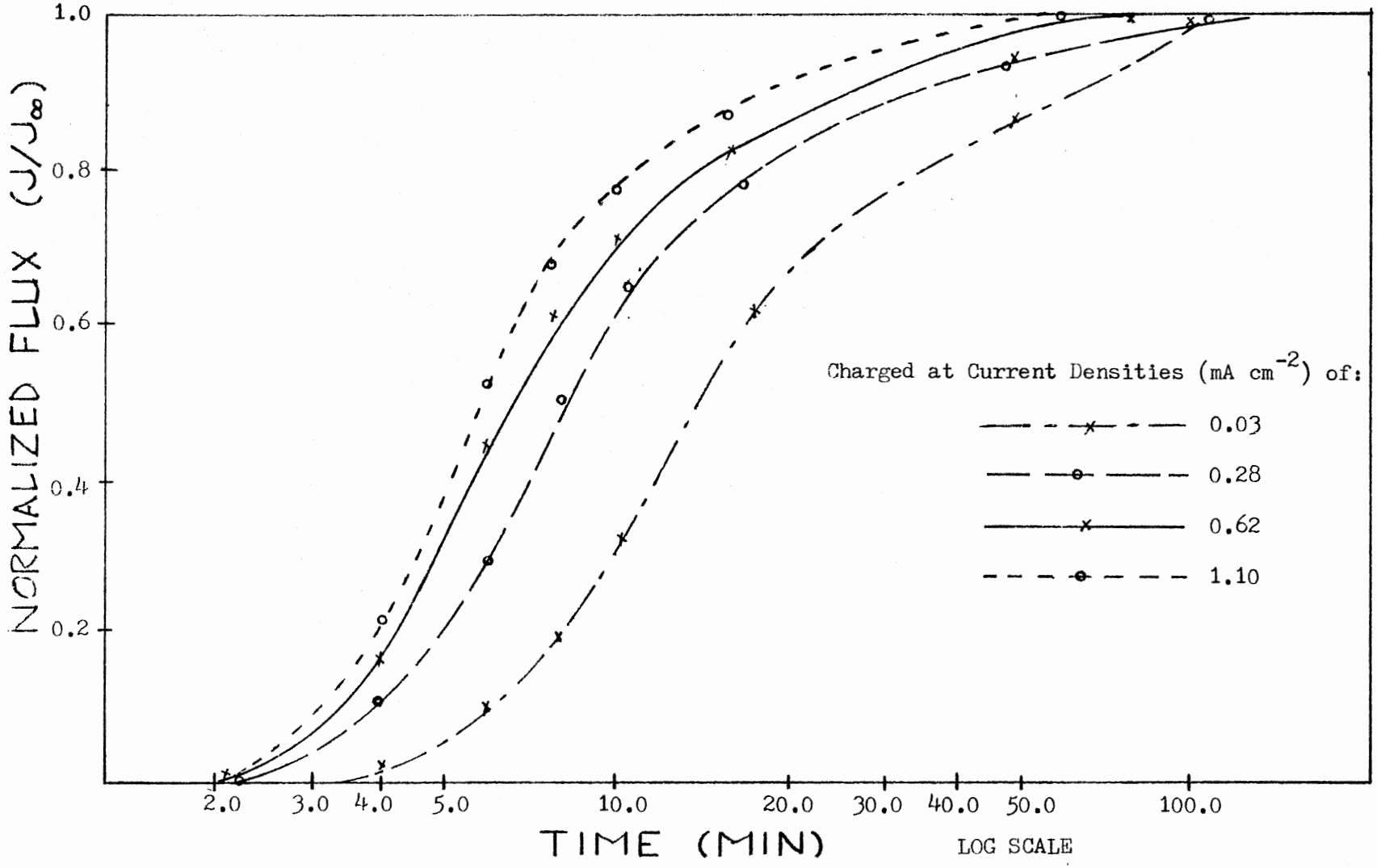

Figure 13. Rise Transients for Cold-Worked Armco Iron.

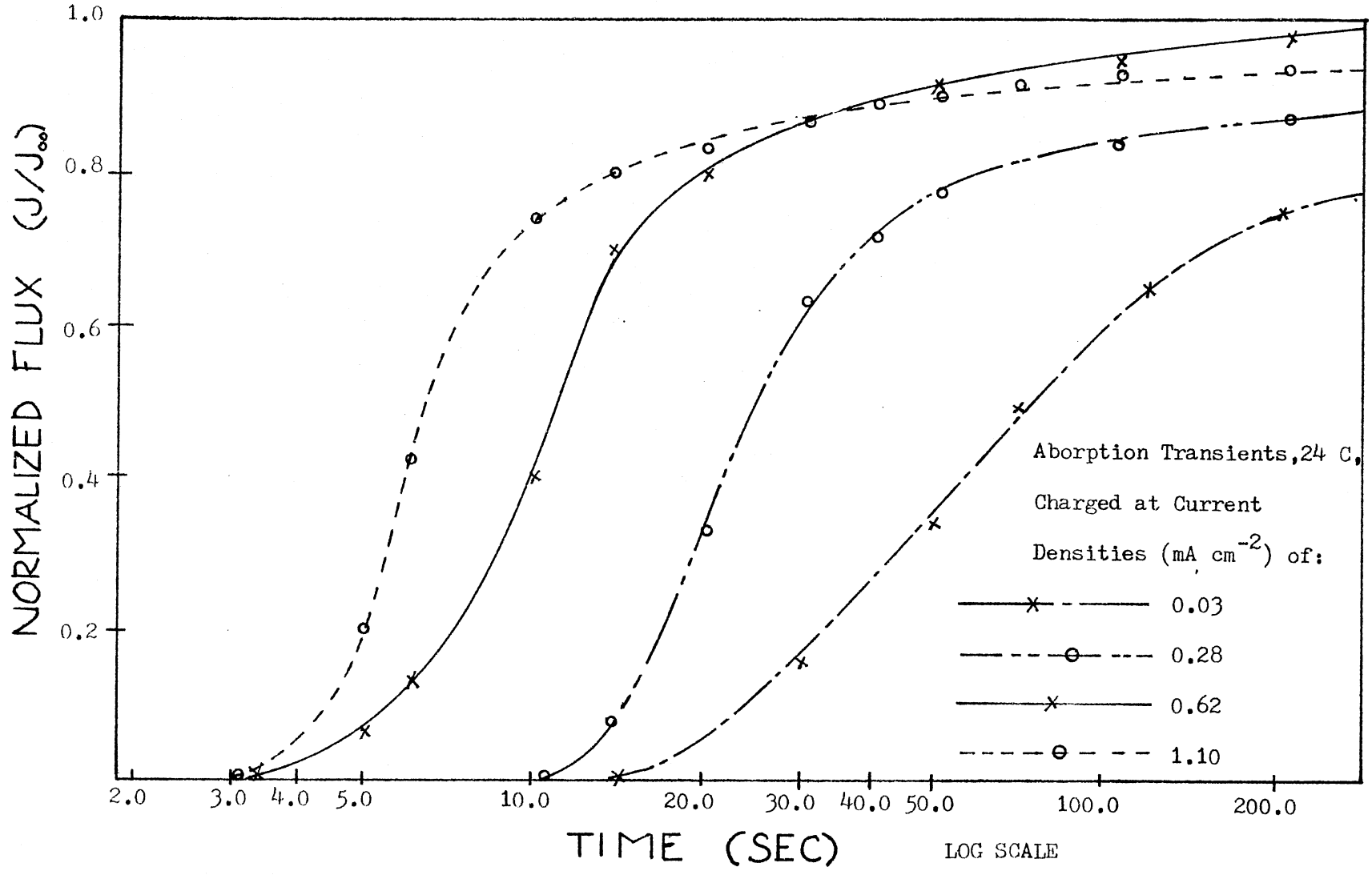

Figure 14. Rise Transients for Annealed 1015 Steel.

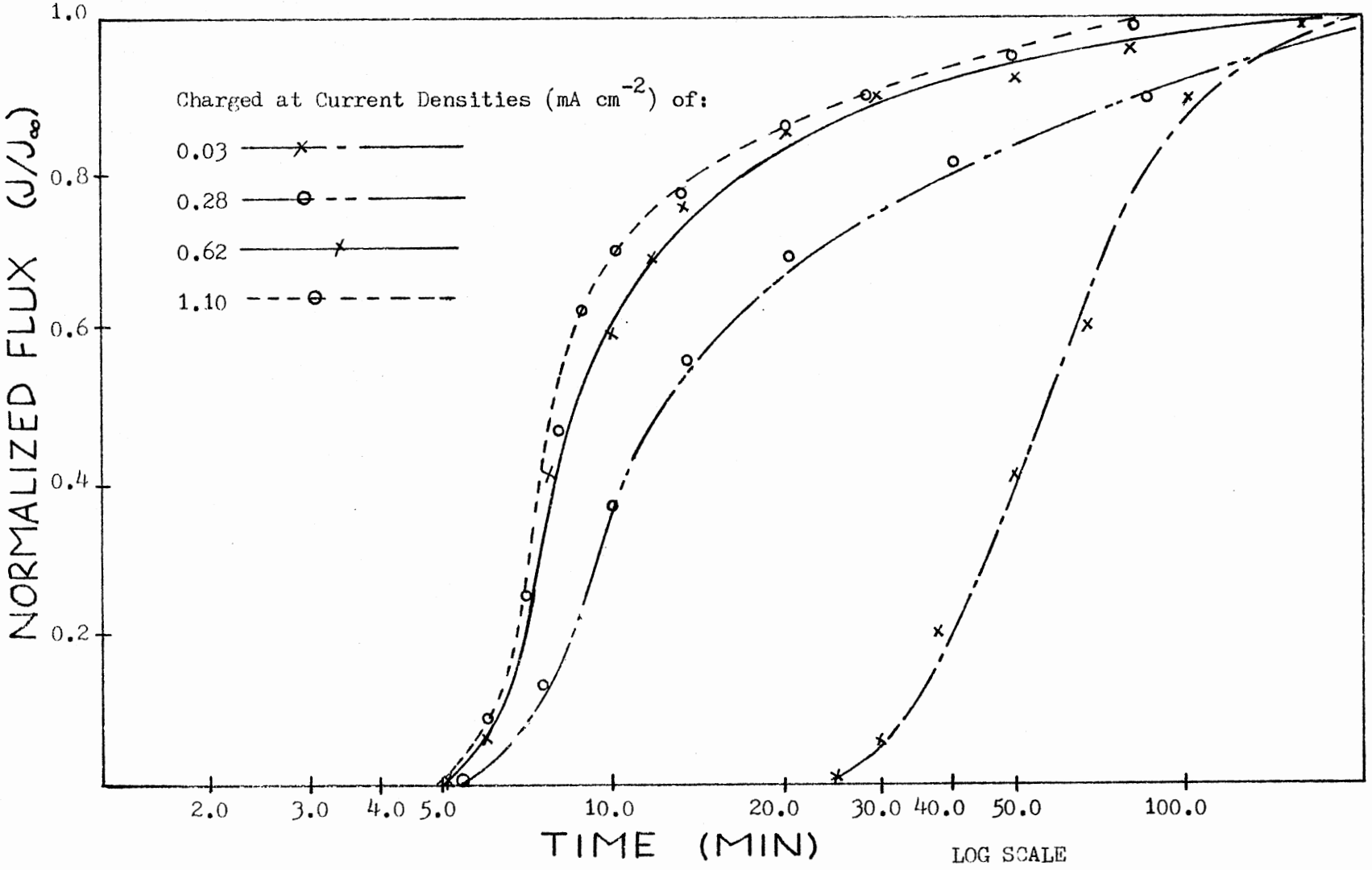

Figure 15. Rise Transients for Cold-Worked 1015 Steel.

TABLE V

COMPILED HYDROGEN PERMEATION DATA FOR
ARMCO IRON AND 1015 STEEL

Specimen and Thickness cm	Charging Current Density ma/cm^2	Steady State Flux, J_∞ $atom\ H/cm^3$ $(\times 10^{-13})$	$C_0^{(1)}$, Input Concentration $atom\ H/cm^3$ $(\times 10^{-17})$	$C_0^{(2)}$, Input Concentration $atom\ H/cm^3$ $(\times 10^{-17})$	Permeability $atom\ H/cm^3$ $(\times 10^{-11})$
Annealed[3] Armco Iron	0.03	1.14	1.72	2.06	2.04
	0.28	3.25	1.85	2.07	5.85
	0.62	4.80	1.11	1.22	8.55
L = 0.018	1.10	6.75	1.30	1.38	12.20
Annealed[3] 1015 Steel	0.03	1.39	3.40	4.80	2.60
	0.28	3.53	3.05	3.46	6.65
	0.62	5.13	2.09	2.38	9.75
L = 0.019	1.10	7.28	1.56	1.79	13.80
Cold Worked[3] Armco Iron	0.03	2.14	41.76	48.65	2.75
	0.28	7.65	73.60	73.02	8.03
	0.62	10.84	75.09	85.41	10.80
L = 0.020	1.10	13.31	97.65	97.60	16.50
Cold Worked[3] 1015 Steel	0.03	2.14	164.10	214.00	4.92
	0.28	7.65	159.91	228.50	17.60
	0.62	10.84	166.02	177.90	30.60
L = 0.023	1.10	13.31	180.12	187.80	30.60
Cold Worked[4] Armco Iron	0.057	6.38	116.00	159.50	12.76
	0.080	8.21	65.72	65.72	16.43
L = 0.020					
Cold Worked[4] 1015 Steel	0.057	14.70	359.04	373.41	37.34
	0.114	22.75	320.89	361.00	57.76
	0.170	30.74	433.74	487.96	78.10
L = 0.025					

(1) Determined using Equation 35 for D_{eff}.

(2) Determined using Equation 36 for D_{eff}.

(3) Charging solution contained 0.1N NaOH.

(4) Charging solution contained 0.1N NaOH + Na_2AsO_4.

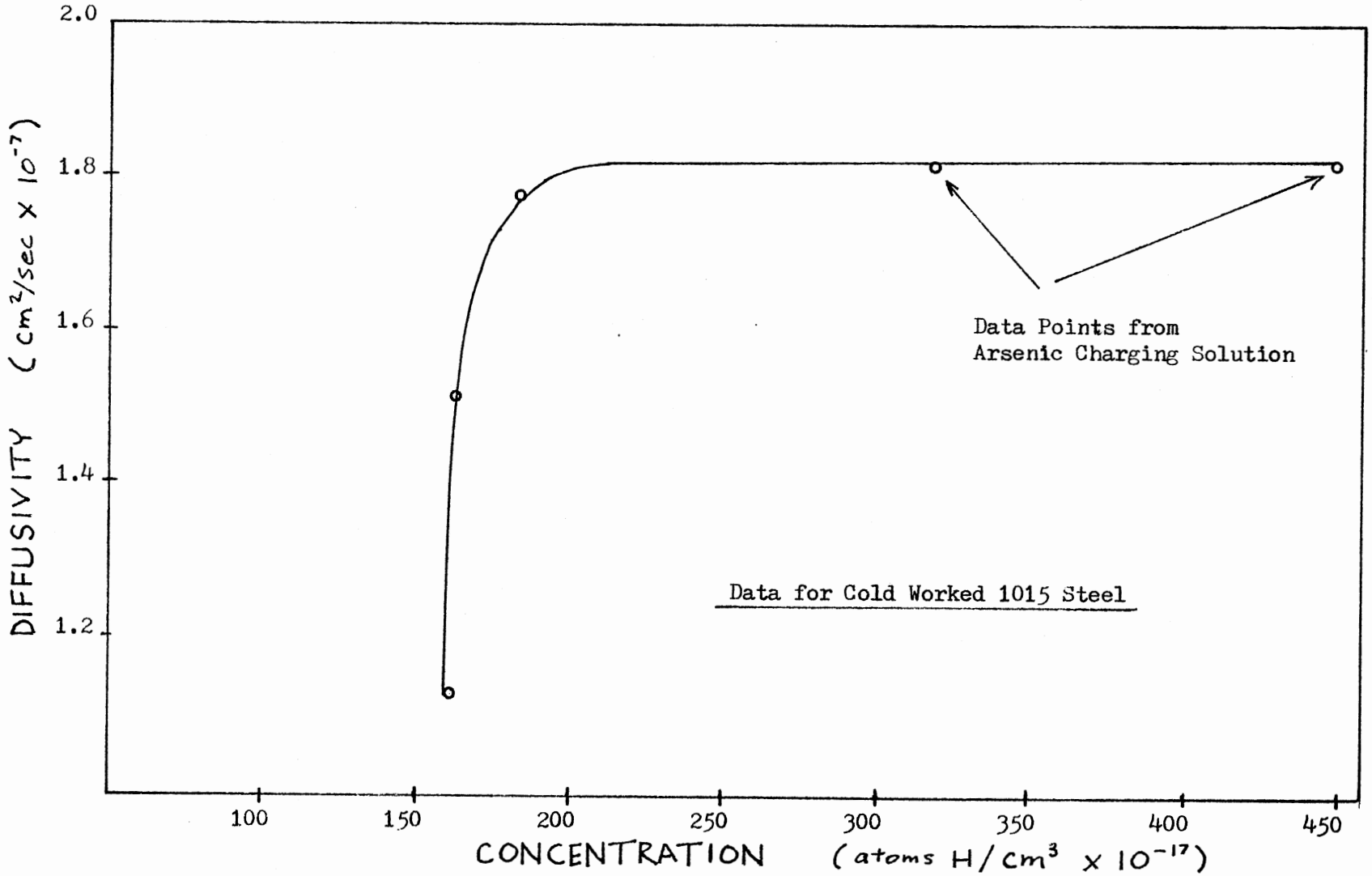

Figure 16. Curve Depicting Hydrogen-Concentration Dependent Diffusivity.

findings might indicate that the effective diffusivity is increasing with lattice concentration due possibly to an increasing fractional occupancy of traps.

The influence of reversible trapping on the absorption transients for Armco iron is shown in Figure 17. Curve 1 depicts lattice diffusion while curves 2 and 3 indicate permeation delay characteristics of trapping in annealed and cold worked iron, respectively. The difference between the lattice diffusion transient and the other experimental transients is a measure of the extent of reversible trapping in the material. The reversible trapping behavior of the Armco iron and 1015 steel is very similar as shown by their diffusivities in Table IV. The lower values of diffusivities of the cold worked materials than those of the annealed materials was thought to be due to the effect of mechanical deformation on the structure of the material. Significant trapping was also indicated in the annealed iron and several estimates were made to identify types of traps in the materials that had a major density or trapping influence.

Possible candidates for trap sites are carbide particles, grain boundaries, dislocations and voids. Since Armco iron has a very low carbon content and inclusion content, these types of traps were not considered to make up a large density. A technique (42) was used to determine the grain boundary area in the annealed iron and steel so that an estimate of the number of hydrogen trap sites per cm^3 could be found. In this technique, the microstructure of the iron was determined. A ruler was placed across the picture and the number of grain boundary intersections with a line of known length was measured. For the annealed iron, the analysis is as follows:

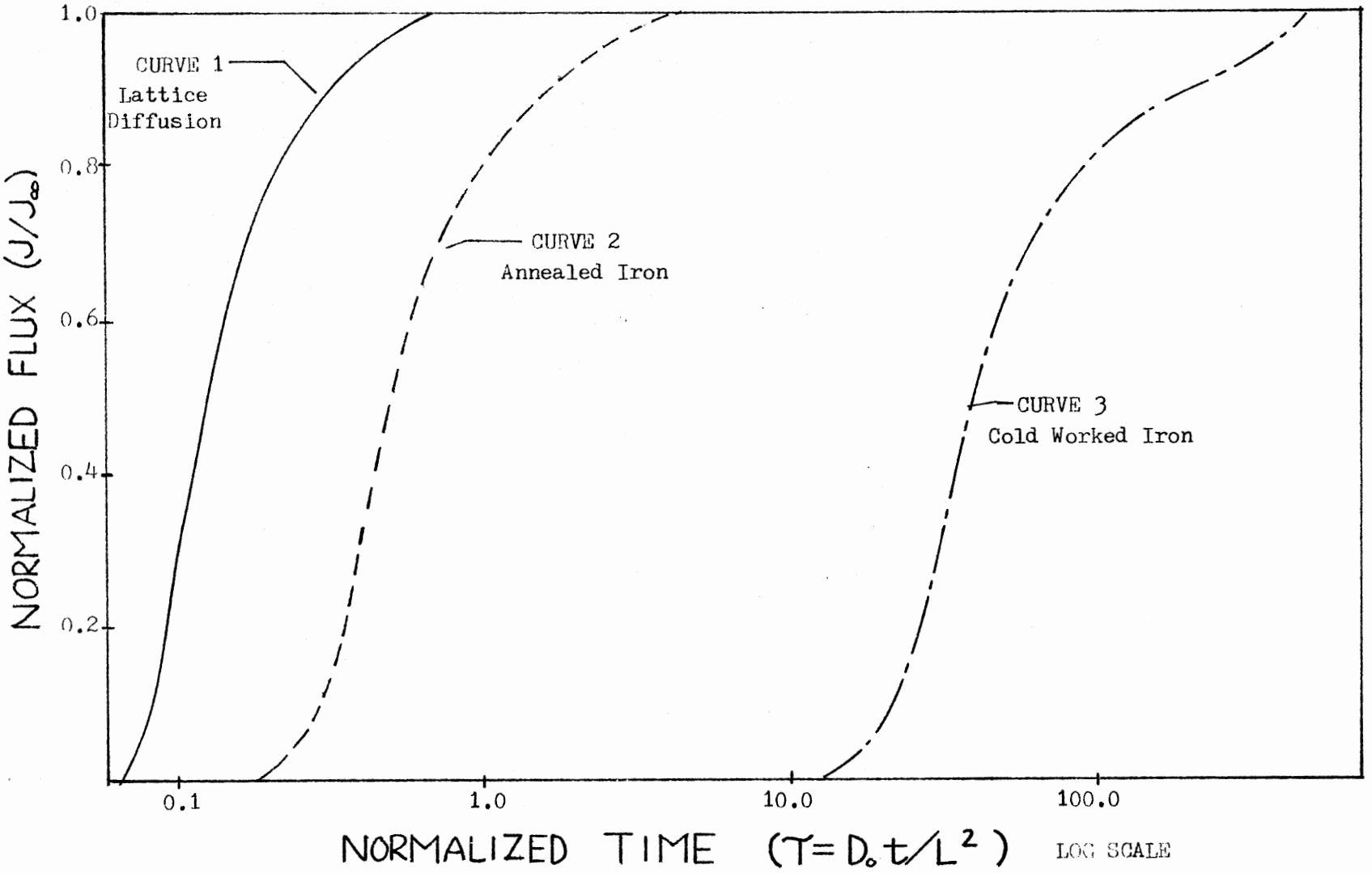

Figure 17. The Influence of Trapping on the Absorption Transients for Iron.

7 grain boundary intersections/9.5 cm

Magnification of photograph = 250 x

P_L = 7 x 250/9.5 = 184.2 grain boundaries/cm

$$Sv = 2\ P_L \tag{27}$$

where

S_V = grain boundary surface area/unit volume

P_L = number of points of intersection per unit length of the line and the grain boundaries

S_V = 369.42 cm^2/cm^3

It is assumed that there is one hydrogen trap site per unit cell on the grain boundary surface. The lattice parameter of bcc ferrite is used as the dimensions of the unit cell. Therefore

$$\frac{368.0\ cm^2/cm^3}{2.87 \times 10^{-8} Mm)^2} \qquad \text{g.b. surface area/unit volume}$$

$$= 4.47 \times 10^{17}\ \text{H traps/cm}^3\ \text{Fe}$$

The cold worked iron should not have a significantly different trap density because the volume of the ferrite grain stays approximately the same during the cold rolling process.

Next, an estimate of the trap density of dislocation was made. The number of dislocation lines (39) in annealed iron and steels is of the order of 10^8 cm/cm^2 and 10^{11} cm/cm^2 for heavily cold worked iron and steels. If it is assumed that there is one hydrogen trap site per atomic plane perpendicular to the dislocation line per volume of materials, then the results are as follows:

trap density - dislocations:

annealed iron and steel -------- 10^{15} $traps/cm^3$

cold worked iron and steel ----- 10^{19} traps/cm^3

Taking the trap binding energies of grain boundaries and dislocations to be approximately the same, as they are reported in Reference 24, it is seen that there is a greater trap density in the cold worked metals attributed to increase dislocation density as the result of deformation.

Values of calculated trap densities, based on permeation data, are given in Table VI for the Armco iron and 1015 steel. To calculate the trap density, N_T Equations 13 and 17 were combined to give:

$$N_T = \left(\frac{Do}{D} - 1\right) (\exp - \Delta E_x/RT) N_o \qquad (28)$$

A trap binding energy for dislocations of 28.0 KJ/mole as given by several authors (24), (29), (28) was used to find one value of N_T from the equation above. Another trap binding energy of 58.6 KJ/mole, as found by Kumnick and Johnson (31) in their analysis of mechanically deformed Armco iron, was also used to find N_T. The values of trap density given in Table VI are calculated by using two different values of diffusivity. A trap binding energy of 28.0 KJ/mole gives very large trap densities (10^{25} - 10^{26} m^{-3}) while a trap binding energy of 58.6 KJ/mole gives lower densities (10^{19} - 10^{21} m^{-3}). The later results agree fairly well with similar determinations (15), (24). The data of Xie and Hirth (32) and Kumnick and Johnson (31) for trap density versus percentage cold work is given in Figure 18. It appears that the trap density of the present study is either slightly higher or slightly lower than the values depicted by Figure 18 depending on the value used for binding energy. Xie and Hirth (32) have suggested that a trap binding energy of 28.0 KJ/mole gives a value of trap density that is too large.

The computer results of the transient analysis are given in Appendix

TABLE VI

TABULATED TRAP DENSITIES FOR
ARMCO IRON AND 1015 STEEL

Specimen and Thickness cm	Charging Current Density ma/cm^2	Trap Density, N_T (cm^{-3}) E_B = 28.0 KJ/mole $N_T^{(1)}$ ($\times 10^{-20}$)	E_B = 28.0 KJ/mole $N_T^{(2)}$ ($\times 10^{-20}$)	E_B = 58.6 KJ/mole $N_T^{(1)}$ ($\times 10^{-14}$)	E_B = 58.6 KJ/mole $N_T^{(2)}$ ($\times 10^{-14}$)
Annealed[3] Armco Iron	0.03 0.28 0.62				
L = 0.018	1.10	0.118	0.129	0.404	.442
Annealed[3] 1015 Steel	0.03 0.28 0.62				
L = 0.019	1.10	0.131	0.165	0.449	0.566
Cold Worked[3] Armco Iron	0.03 0.28 0.62				
L = 0.020	1.10	9.730	9.730	33.300	33.300
Cold Worked[3] 1015 Steel	0.03 0.28 0.62				
L = 0.023	1.10	9.730	10.010	33.000	34.800
Cold Worked[4] Armco Iron	0.057 0.080				
L = 0.020		6.590	6.590	22.600	22.600
Cold Worked[4] 1015 Steel	0.057 0.114 0.170				
L = 0.025		9.180	10.300	31.500	35.540

(1) Determined using Equation 35 for D_{eff}.

(2) Determined using Equation 36 for D_{eff}.

(3) Charging solution contained 0.1N NaOH.

(4) Charging solution contained 0.1N NaOH + Na_2AsO_4.

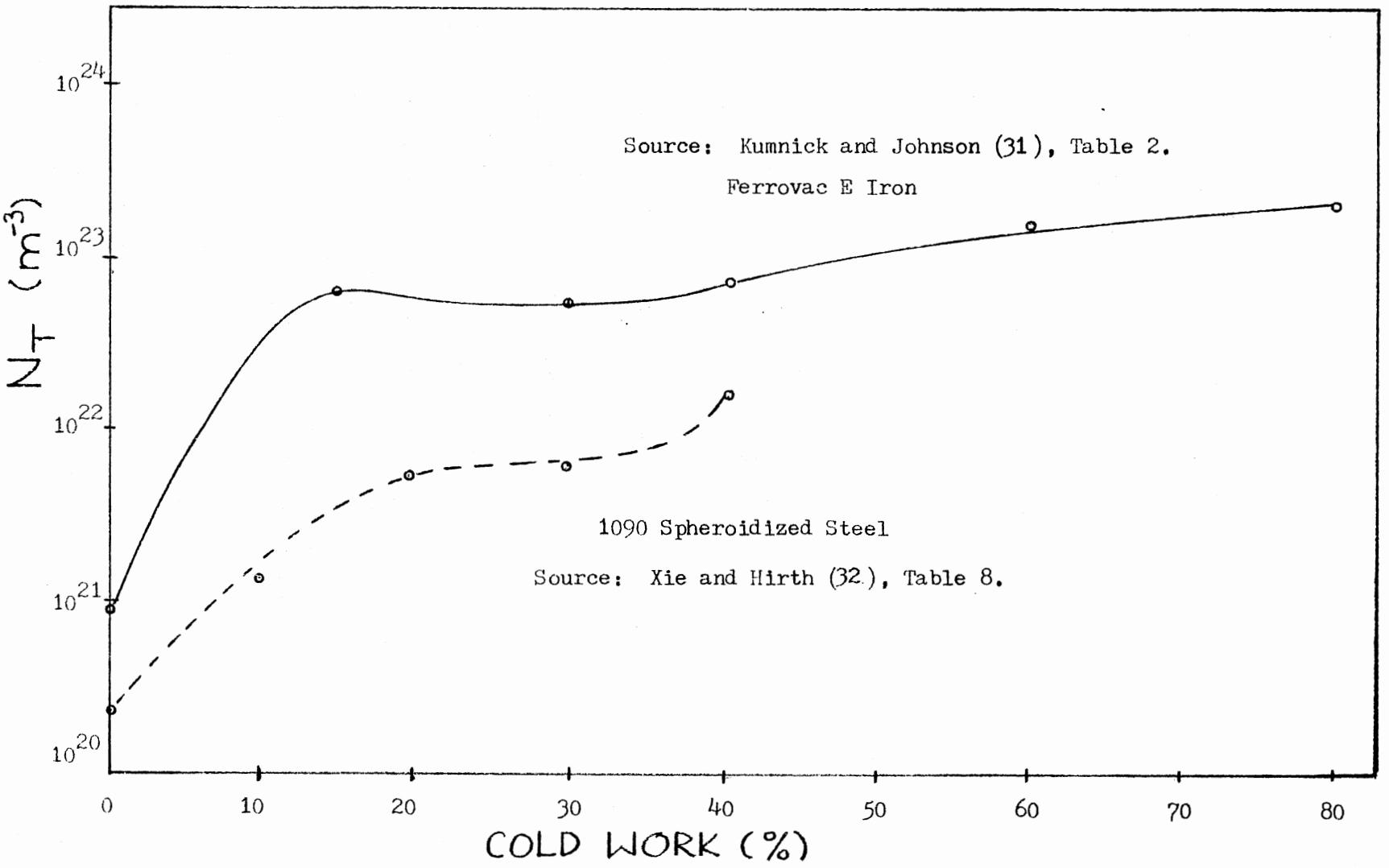

Figure 18. Trap Density Versus Percent Cold Work for Ferrovac E Iron and Spheroidized 1090 Steel.

B. Figure 19 shows numerical solution curve fit to the experimental transient for annealed and cold worked iron. The computer curve-fitting parameters, trapping parameters and the results of the computer analysis are given in Table VII. These results show a trap density of 9×10^{13} cm^{-3} for annealed iron and a trap density of 6×10^{15} cm^{-3} for cold worked iron. A unique solution to the various trapping parameters was not obtainable because the relationship between D/D_o, λ/μ and λ/ν in Equations 9, 19 and 20 did not hold for the experimental data in this study. However, by assuming a trap binding energy, the other parameters could be obtained. A trap binding energy, E_B = 28 KJ/mole, was found to give large values of trap density $10^{17} - 10^{19}$ cm^{-3}, while E_B = 58.6 KJ/mole gave trap densities of $10^{13} - 10^{15}$ cm^{-3}. Several authors (31), (32) have suggested that the lower value of trap binding energy gives trap densities that are excessivly large and so E_B = 58.6 KJ/mole was taken to be the best value of binding energy. The computer output data also consisted of the determination of the lattice and trapped hydrogen concentration profiles through the thickness of the membrane. The concentration profile for cold worked iron at steady state conditions indicated that the relative trapped concentration was larger than the relative lattice concentration by a factor of approximately 300. This result indicates that a large percentage of hydrogen in the metal during the diffusion process was immobilized by traps.

The effect of arsenic on hydrogen permeation is shown by the absorption transient in Figure 20. The permeation transients described by Figure 20 show the permeation current to increase and reach a maxima at a point where it then suddenly decreases. This bowing down of the absorption transient curve occurred even though a steady charging current was being

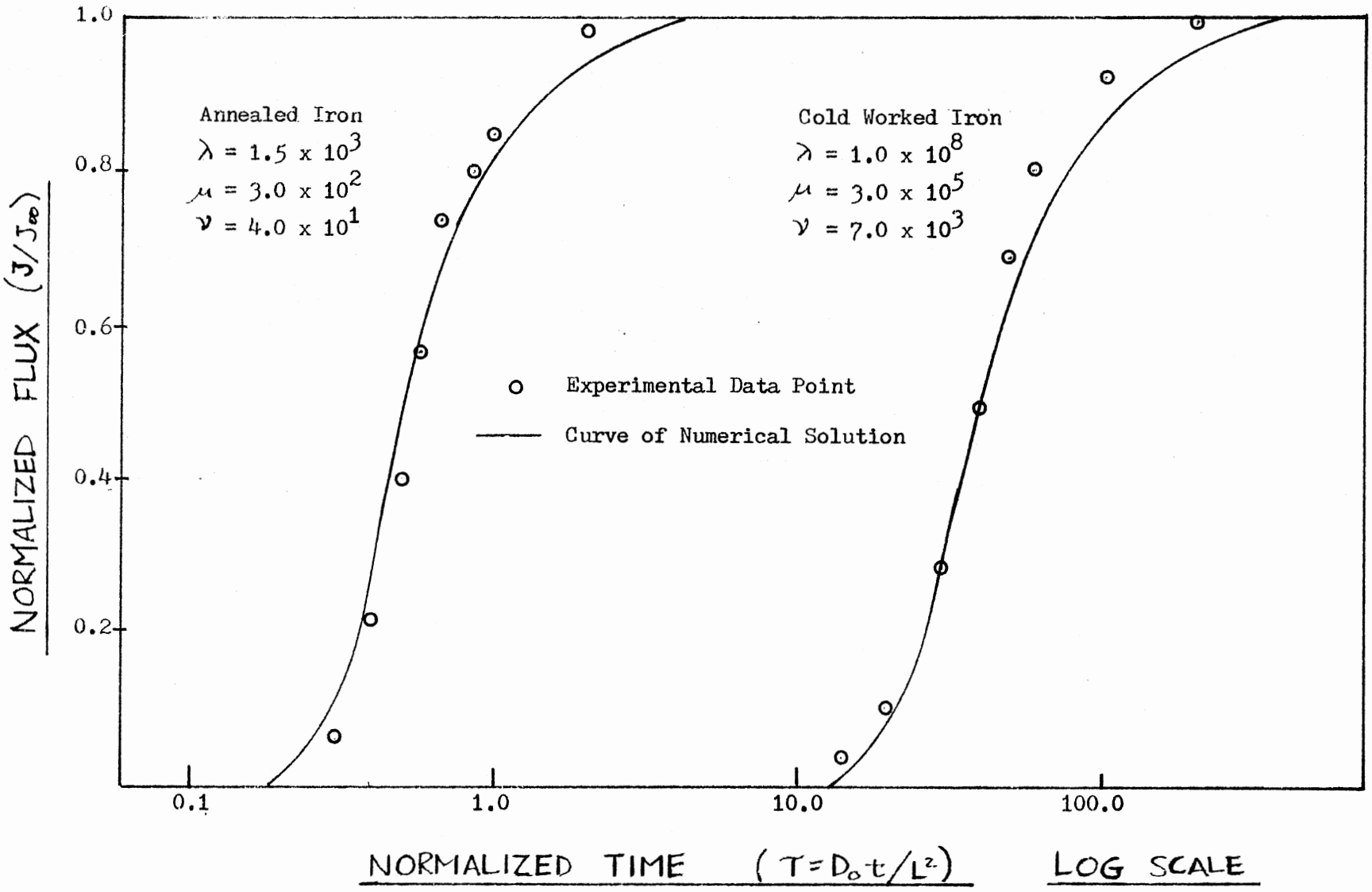

Figure 19. Transient Analysis and Curve Fitting Parameters.

TABLE VII

RESULTS OF TRANSIENT ANALYSIS

Specimen Charging Density, I_c (ma/cm^2)	Curve Fit Computer Parameters			Trapping Parameter		Trap Binding Energy E_B KJ/mole	Trap Density N_T cm^{-3} ($x10^{-14}$)	Steady State Trap Occupancy	Steady State Trapping Rate	Steady State Release Rate
Annealed Armco Iron	1.5×10^{3}	3.0×10^{2}	4.0×10^{1}	2.87×10^{2}	1.58×10^{-12}	58.6	0.91	0.118	3.07×10^{14}	3.07×10^{14}
L = 0.018										
I_c = 0.62										
Cold Worked Armco Iron	1.0×10^{8}	3.0×10^{5}	$7.0\ 10^{3}$	2.33×10^{4}	1.28×10^{-9}	58.6	60.60	0.023	3.28×10^{18}	3.28×10^{18}
L = 0.020										
I_c = 0.62										

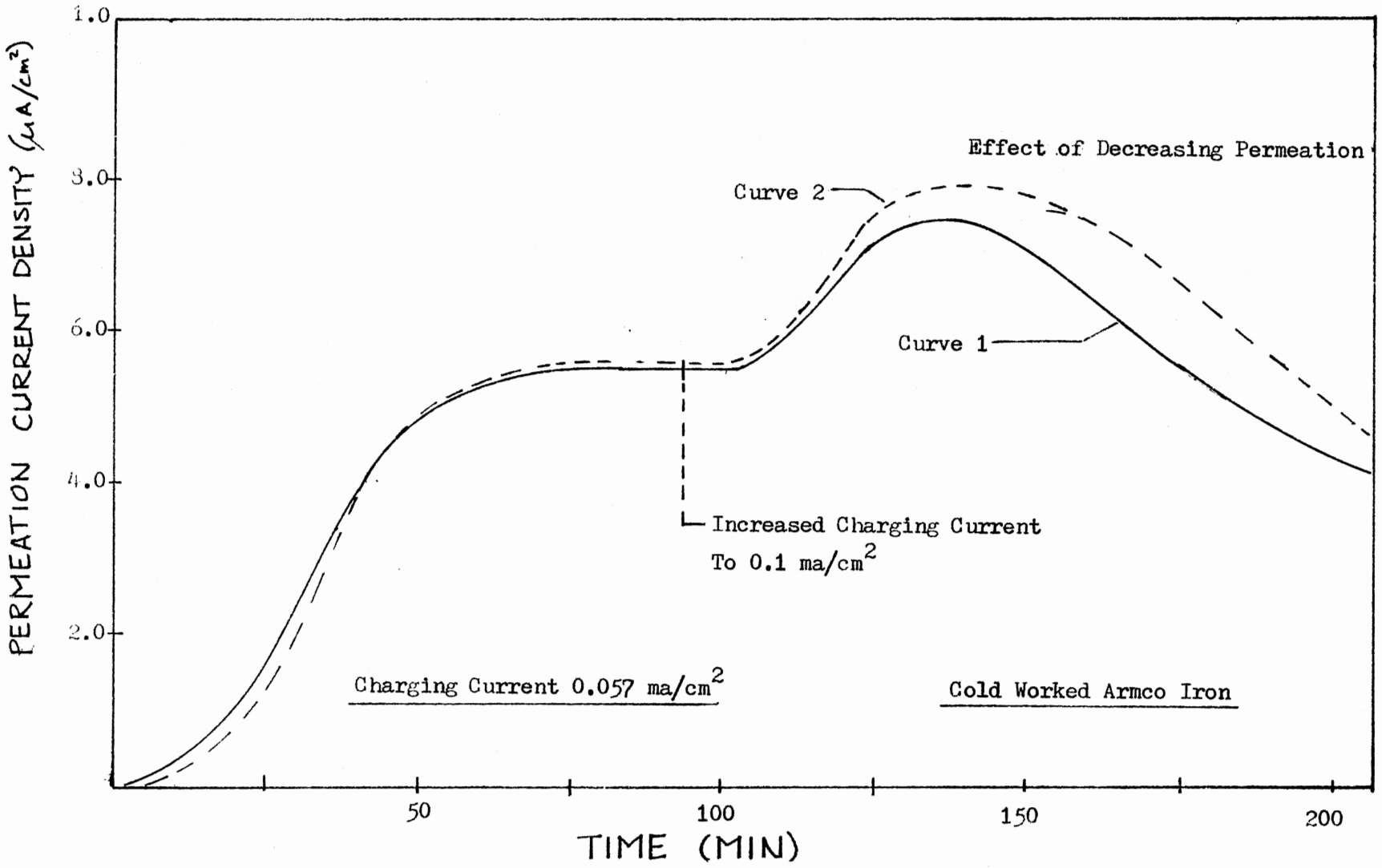

Figure 20. Effect of Arsenic on the Absorption Transient for Cold-Worked Armco Iron.

applied, indicating that hydrogen permeation was decreasing. Surface inhibition of the membrane was initially suspected as causing the decrease in permeability. The iron membrane was examined for visible evidence of an inhibiting scale formation on the surface but none was found. The next day, the same sample was charged again, and the resulting absorption transients are shown by Curve 2 in Figure 20. The transient produced by the charging current I_c = .057 ma/cm^2 was found to be reproducible with the transient obtained the previous day. However, the same effect of decreasing permeation occurred at the higher charging current I_c = 0.1 ma/cm^2. The unusual permeation behavior suggested that either inhibition of the membrane surface or internal damage to the membrane was occurring. Xie and Hirth (32) found that when a critical charging current density is reached, blisters can form in the material. These authors calculated the hydrogen fugacity at the surface of the membrane and then determined the equivalent molecular hydrogen pressure at this surface. They found that a critical charging current density corresponding to a pressure of 2/3 of the yield strength of the steel would cause blister nucleation in the steel. Xie and Hirth's analysis will be lowed to determine if the charging currents used in the study were high enough to create blisters in the Armco iron. permeation data from the present study was used in Equation 32 to find the hydrogen surface concentration, C, as follows:

Permeation current = 7.65 μ A/cm^2

Permeation flux = 7.956 x 10^{-11} moles H/cm^2

D = 6 x 10^{-6} cm^2/sec

L = 0.02 cm

Equation 32 $\quad C = \frac{JL}{D}$ = 0.265 mol H/m^2

From Xie and Hirth (32), Table VII, the fugacity found from C is approximately 1.02 x 10^4 atm. This fugacity corresponds to a molecular hydrogen pressure of about 200 MPa. According to this analysis, a hydrogen surface concentration corresponding to a hydrogen pressure of 200 MPa is indeed enough to create blisters in the metal since the yield strength of cold worked iron is approximately 180 MPa.

B. Discussion

The optimum anodic potential -300 mv (SCE) necessary to oxidize permeating hydrogen was found to be in agreement with that reported by others (35), (36). Devanathan and Stachurski (35) have demonstrated, as have Atrens et al., (36), that an optimum applied anodic potential exists between -600 to -300 mv (SCE) such that rapid ionization of permeating hydrogen will occur on palladium surfaces. Both authors used the largest anodic potential of -300 mv (SCE) during permeation experiments, the same value used in the present study. Kumnick and Johnson (29) imposed a hydrogen-oxidizing potential of +100 mv (SCE) on palladium coated membranes. Examination of the Pourbaix diagram for palladium (37) shows this potential to be very close to the region where anodic dissolution of palladium can occur. Surkein (38) also reported using a relatively high oxidizing potential, +250 mv (SCE), and he found that steady state permeation was never obtained during a 100 hour permeation experiment. He gives a possible explanation of the non-steady state condition as being due to continuous internal damage to the membrane and to the consequential trap growth. A very low charging current was employed in his permeation experiment, 0.025 ma/cm^2, which suggests that the hydrogen fugacity was not high enough to create damage to the membrane.

Surkein's results, based on the oxidizing potential he used, indicate that the membrane was corroding during the experiment. Increased corrosion current led to increased steady state permeation current.

The effectiveness of the plating process in the present investigation was demonstrated by the quality of the palladium coating. The electrochemically-deposited-palladium coatings used in the study were microscopically inspected before and after each permeation experiment and found to be free of surface defects; i.e., absence of holidays. A typical palladium coating on an Armco iron specimen was examined by a scanning electron microscope and the surface was found to be featureless and non-porous. Heidersbach et al., (43) reported that the palladium coating is intended to produce an inert surface, minimizing corrosion effects on hydrogen entry, while supplying a readily permeable medium which is not rate controlling for hydrogen transport.

Qualitatively, the results of Figure 9 are in close agreement with the expression given by Bockris (40) that steady state hydrogen flux is proportional to the square root of the changing current for hydrogen permeation in 0.1N NaOH charging solutions. Mathematically, this effect can be expressed through thermodynamic relationships that describe the rate and the energetics involved in the adsorption, transport and desorption of hydrogen in the diffusion process. The following electrochemical reactions describe a possible basic mechanism for the hydrogen evolution reaction (36):

overall reaction

$$2H_2O + 2e^- \longrightarrow H_2 + 2OH^- \quad \text{(in alkaline solutions)} \qquad (29)$$

is split into elementary steps, which are for alkaline solutions

$$M + H_2O + e^- \longrightarrow MHads + OH^- \quad \text{(discharge)} \qquad (30)$$

$$MHads + MHads \longrightarrow H_2 + 2M \quad \text{(recombination)} \tag{31}$$

$$MHads + H^+ + e^- \longrightarrow H_2 + M \quad \text{(electrochemical desorption)} \tag{32}$$

The discharge step occurs first followed by recombination or electrochemical desorption. The rates at which these steps occur are very important in the mathematical treatment of the hydrogen entry, transport and desorption process. It has been demonstrated that there are six possible models for the hydrogen evolution reaction (36).

The electrochemical reactions given above can be used, in a basic way, to describe the effect of arsenic on the permeation current-charging current relationship. The chemisorption of arsenic on the surface lowers the metal-adsorbed hydrogen bond (M-Hads) and allows greater hydrogen surface coverage (40). The rate of hydrogen adsorption and entry is increased, thereby increasing the permeation rate. The desorption step is suggested to be electrochemical instead of combination for higher overpotentials (40). The drastic effect of arsenic on hydrogen permeation behavior is shown in Figures 8 and 10. The linear relationship between permeation current and charging current for the arsenic solution indicates higher kinetic reaction rates are occurring in the hydrogen evolution reaction and are reflected in higher permeation currents.

The concentration dependent diffusion observed in this study is difficult to explain based on the model (15) that local equilibrium exists between trapped and diffusing hydrogen. If local equilibrium exists, the trapped concentration should be linear to the lattice concentration as trapping and untrapping keep pace with the rise in local concentration. Oriani's condition (15) for local equilibrium assumes that when there is a small fraction of occupied traps the effective

diffusivity does not depend on the lattice concentration. It appears that during the permeation experiment that a large fraction of traps are actively involved in the diffusion reactions. In this case, Equations 9 and 11 cannot be used to describe this process because the local equilibrium condition is invalidated. Oriani has also indicated, however, that when sufficient trapping sites are involved in the diffusion process, the experimental value of diffusivity will be a function of the concentration of diffusing hydrogen. Equation 12 can be used to employ diffusivity changes in this case. Namboodhiri and Nanis (41) found the diffusivity of hydrogen in Armco iron to increase linearly with increased hydrogen surface concentration. From their data of diffusivity versus hydrogen concentration, they have drawn a straight line through the data points suggesting the linear relationship. Their data shows considerable scatter, and it is found that values of diffusivity for the same hydrogen concentration values differ by a factor of two. the data shown could seemingly be presented as shown in Figure 16 where the hydrogen diffusivity actually reaches a limiting value and does not depend on further increases in concentration. The present results seem to indicate that the effective diffusivity is increasing due to an increasing fractional occupancy of traps. At a limiting value of hydrogen concentration, the difference between trapping and de-trapping rates becomes smaller. Further, at high hydrogen concentrations, a relatively higher amount of hydrogen is available for lattice diffusion even after trapping has taken place. These effects can account for concentration independence of diffusivity above a limiting value of hydrogen concentration. It must also be noted from Figure 16 that the concentration dependent diffusivities are in a relatively small range.

Armco iron and 1015 steel showed similar trapping behavior in both the annealed and cold worked state. The pronounced effect mechanical deformation has on hydrogen permeability in the materials is evident from Table IV which shows the diffusivity of hydrogen in the cold worked material is decreased by a factor of about 50 from the diffusivity value for the annealed material. Several different types of trapping sites were investigated to determine which trap type exerted a major influence on trapping.

The densities associated with grain boundary trapping sites were shown to be negligible for the Armco iron and steel. These results are in agreement with those of Bockris (40) and Beck et al., (34) who found that in both single crystal and polycrystal Armco iron grain boundaries play no major part in the diffusion of hydrogen in the iron. Beck et al., (34) also demonstrated that for polycrystalline Armco iron and zone refined iron trace impurities had no effect at all on hydrogen diffusion.

Oriani (15) has reported the increase of trap density with increasing carbon content and strength level in steels. Typically, 1015 steel would have a large density of trapping sites at internal interfaces because of the presence of carbides, nitrides and other second-phase particles. Hydrogen, in the same way as nitrogen, has been demonstrated to be strongly adsorbed at the interface between Al N particles and ferfite (44). Lacombe et al., (26), as discussed earlier, found strong binding energies (60 KJ/mole) for hydrogen at such solid-solid interfaces. Normalized 1015 steel has a large interfacial area per unit volume material at ferrite-cementite boundaries. The extent of the internal interface area and the corresponding number of trap sites were determined

for the 1015 steel used in this study. However, Oriani (15) calculated a trap density of 3.5×10^{19} cm^{-3} for a 0.1% carbon steel and 2.8×10^{20} cm^{-3} for a 0.8% carbon steel. This analysis was based on a ferrite-cementite interfacial area of 10^4 cm^2/g for a pearlitic steel of 0.8% carbon. The hydrogen sites were assumed to be at the octahedral interstitial positions in the (100) plane of the ferrite-side interface. Solid-solid interfaces have been considered as the predominant trapping site for hydrogen in steels that have not been cold worked (15), (26). Armco iron, with its low impurity concentrations, is not expected to have a large particle-interface volume; however, the diffusion behavior of hydrogen in Armco iron and 1015 steel has been shown to be similar in this study. The above findings suggest that interfacial trapping sites in the 1015 steel are either traps of an irreversible nature, and/or very shallow traps that do not influence hydrogen diffusion to a significant degree. Again, these findings support the evidence that the typical impurity concentrations of a 1015 steel do not significantly reduce the effective diffusivity of hydrogen in the steel as compared to the diffusivity of hydrogen in a more pure metal, Armco iron. Also, the fact that the difference between the effective diffusivities calculated for first and second permeation transients are higher for the 1015 steel, unequivically support the conclusion that the major role of carbide/particle-matrix interfaces is in irreversible trapping. Thus, reversible trapping has to be explained by trapping, the nature of which is extraneous to particle/matrix interfaces.

The findings in the present study are similar to the findings reported by Kumnick and Johnson (29) of the effect of mechanical deformation of hydrogen trapping and permeability in Armco iron. These authors plotted values of diffusivity versus percent cold work for Armco

iron. The values of hydrogen diffusivity for the Armco iron used in the present study corresponded to a value, from the plotted curve, of 30% reduction. Since the actual value of cold work was not known for the Armco iron, it is not possible to discuss the accuracy of this method in determining cold work for our specimen. Kumnick and Johnson (29) considered two major types of reversible traps in the Armco iron, microvoids and dislocations. They found that microvoids are thermally stable traps, and they do not disappear or decrease in volume at annealing temperatures. They demonstrated that since there was no significant change in density of the Armco iron upon rolling to a 75% reduction in thickness, that microvoid traps were negligible compared to dislocation traps. They used McNabb and Foster's equation (14) for saturation of traps to calculate a trap density of 2.7×10^{16} cm^{-3} for 40% cold worked Armco iron. The values of trap density recorded in Table VI show similar results. Based on the above discussion of trapping sites in Armco iron and 1015 steel, it is concluded that the major reversible traps in cold worked Armco iron and 1015 steel are dislocations, in excellent agreement with other observations (15), (21), (27), (29).

It is evident from Table VI that a trap binding energy, E_B = 28.KJ/mole, gives rather large values of trap density (10^{19} to 10^{15} cm^{-3}) and a trap binding energy, E_B = 58.6 KJ/mole, gives smaller values of trap density (10^{13} to 10^{15} cm^{-3}). The average difference between each of these two sets of trap densities is 10^{6} cm^{-3}. Obviously, there is a significant discrepancy in the correct value of E_B since both values E_B are associated with hydrogen-dislocation trapping sites in iron. It was assumed earlier in this thesis that a maximum dislocation density of 10^{11} cm/cm^{2} for a heavily cold worked steel would yield up to 10^{19}

hydrogen traps/cm^3. Chou and Li (44) assigned 5 trapping sites per dislocation line per atomic plane to calculate a trap density of 3.5 x 10^{19} cm^{-3}. They considered hydrogen being held in the stress fields of dislocations. Kumnick and Johnson (29) have suggested trap densities of the order 10^{16} cm^{-3} are associated with non-elastic trapping sites along dislocation cores or with point debris left behind by moving dislocations during mechanical deformation. Kumnick and Johnson ruled out elastic trapping of interstitials or solute atmospheres around dislocations because high stresses would be required to trap hydrogen. However, Hirth and Carnahan (45), in their analysis of dislocation trapping theory, calculated binding energies from dilational strain around dislocations to be about 41.8 KJ/mole, a significant trap binding energy. The contribution of the remote stress field atmosphere to the apparent enhancement in hydrogen solubility was estimated to be a moderate one. An enhancement factor of 6.1 was cited for a dislocation density of 1.16 x 10^{15} m^{-2}. In view of the above discussion, it would appear that dislocation trap densities of the order of 10^{16} cm^{-3} for cold-worked iron and steel would be a more practical assessment of trap densities. Trap binding energies of the order of E_B = 58.6 KJ/mole have been associated with the above mentioned trap densities (25), (31) and are in agreement with the analysis in this study.

Transient analysis by the McNabb-Foster method (14) yielded important information concerning the trapping behavior of hydrogen in the annealed and cold worked Armco iron. The use of the local equilibrium method to evaluate trapping parameters was shown to be a valid method. Steady state trap occupancy for the annealed iron was

n_s = 0.118 and for the cold worked iron n_s = 0.023. Oriani's condition (15) for local equilibrium requries that the trap occupancy be approximately less than n_s = 0.10. Kumnick and Johnson (31) used the McNabb-Foster time lag method to evaluate trapping in zone refined Ferrovac E iron because during gas phase charging saturation of traps occurs. Their analysis showed n_s = .992 at 0.01 atm hydrogen gas pressure. These authors also found a binding energy of 59.9 $\pm$ 4.6 KJ/mole H and trap densities of 10^{14} to 10^{17} cm^{-3}. They also reported that annealed and deformed iron have the same trap binding energy. The binding energy was shown by these authors to be independent of temperatures and amount of plastic deformation, suggesting a single trap site is represented in the data. The results of the transient analysis found in this study are presented in Table VII. The trap density of annealed and cold worked Armco iron are similar to those reported by Kumnick and Johnson (31). The binding energy used in the analysis of the trapping parameters was 58.6 KJ/mole, similar to the value found by Kumnick and Johnson in their study. In both diffusion processes, for annealed and cold worked Armco iron, the calculated trapping rates were similar to the trapping rates in each material at steady state conditions. These results indicate that at steady state local equilibrium between the trapped and diffusing hydrogen has occurred. At steady state permeation, a constant concentration gradient has occurred in the material as would be expected.

It is concluded that the results of the electrochemical charging technique and the McNabb-Foster transient analysis method has yielded results similar to those obtained by Kumnick and Johnson. Kumnick and Johnson (31) used gas phase charging and the McNabb-Foster time lag

analysis to determine hydrogen trapping and permeation in iron. Lin (25) has shown in his hydrogen permeation studies that the two techniques mentioned above for analyzing hydrogen trapping and permeation behavior in Ferrovac E iron gave results similar to those of Kumnick and Johnson and to the results obtained in this study, again verifying the consistency and agreement of results.

CHAPTER V

CONCLUSIONS

1. Reproducibility of transients indicated effective and successful operation of the electrochemical cell and that internal damage or external corrosion of the membrane was not occurring during the permeation experiments.

2. The procedure used to coat the membranes with electrodeposited palladium was found to give reproducible and nonporous coatings.

3. An anodic potential of -300 mv(SCE) was found to be the optimum potential where complete oxidation of permeating hydrogen would occur and where anodic dissolution of the membrane would not occur. This finding is in excellent agreement with other findings reported in the literature.

4. The effect of arsenic on increasing hydrogen absorption and permeation was demonstrated. A linear relationship was found to exist between charging current and permeation current for specimens charged in the arsenic solution.

5. For specimens charged in 0.1 N NaOH, it was demonstrated that the permeation current was proportional to the square of the charging current; this effect is in agreement with that reported in the literature.

6. Hydrogen damage, as internal blisters, was suggested to have occurred in cold worked Armco iron as the result of charging in an

arsenic charging solution. Present results suggest that a critical current density corresponded to a critical hydrogen fugacity that was sufficient to cause void growth by plastic deformation. The results from the analysis of post permeation behavior correlated well with that found in the literature.

7. Irreversible trapping was found in both Armco iron and 1015 steel. The extent of irreversible trapping was greater in the 1015 steel than in the Armco iron as shown from the lower hydrogen diffusivity in the 1015 steel. Based on first and second transients, carbide/particle-matrix interfaces were deduced as being the major irreversible traps in 1015 steel.

8. A mild concentration dependent diffusivity was observed in Armco iron and 1015 steel. However, the diffusivity became concentration independent with increasing concentration. This effect was suggested to be due to the decrease in the difference of trapping and de-trapping rates with increasing hydrogen concentration, leaving relatively higher amounts of hydrogen available for lattice diffusion.

9. Hydrogen permeation behavior of the second transients revealed significant reversible trapping in Armco iron and 1015 steel. The reversible trapping behavior of both materials was found to be only a function of material state rather than composition or microstructure, thus, there was a difference in trapping in the annealed and cold worked materials.

10. Trapping sites in the Armco iron and 1015 steel that were siscounted as being major reversible traps were grain boundaries, particle-matrix interfaces, inclusions and voids. The trapping influence of these hydrogen trapping sites was based on calculations of trap

densities and trap binding energies and from other findings reported in the literature.

11. Major internal reversible traps in Armco iron and 1015 steel were deduced to be associated with dislocations in the material. The cold worked materials exhibited lower diffusivities than the annealed materials, and this is primarily believed to be due to increased dislocation trapping sites. Calculated values of trap densities correspond well with reported values of dislocation densities in annealed and cold worked iron and steel. Calculated trap densities, 10^{13} - 10^{15} cm^{-3}, and trap binding energy, 58.6 KJ/mole, for dislocation traps agreed well with those values reported in the literature.

12. A numerical solution developed by Caskey and Pillinger based on the McNabb- Foster model was employed in the analysis of experimental absorption transients. The results of the analysis yielded trap densities of 9×10^{13} cm^{-3} for cold worked Armco iron. A trap binding energy of 58.6 KJ/mole was assumed in the analysis because it gave values of trapping parameters that correlated well with other published results.

BIBLIOGRAPHY

1. Kelley, James H., Escher, William J. D. and Deelen, Win Van. Chem. Engr. Prog., 78 58 (1982).

2. Williams, L. O. Hydrogen Power, Permagon Press, Inc., New York (1980).

3. McAuliffe, C. Hydrogen and Energy, Gulf Publishing Co., Houston (1980).

4. Veziroglu, T., Fulki, K., and Ohta, T., eds. Proceedings of the 3rd World Hydrogen Energy Conference, Tokyo, Japan 1980. Hydrogen Energy Progress, Permagon Press, New York (1981).

5. Metals Handbook. "Failure Analysis and Prevention." Vol. 10, 8th Edition, American Society for Metals, Metals Park, Ohio, (1975), pp. 232-233.

6. Gray, H. R. ASTM Special Technical Publication 543, American Society for Testing and Materials, Philadelphia, Pa., 1972, pp. 3-138.

7. Chandler, W. T. and R. J. Waher. "Hydrogen-Environment Embrittlement of Metals and Its Control." The Hydrogen Economy Miami Energy (Theme) Conf., editor: Veziroglu, T., Permagon Press, NY (1974), pp. S5-13, S6-14.

8. Laws, J. S., V. Frick and J. McConnell. "Hydrogen Gas Pressure Vessel Problems in the M-1 Facilities." NASA Report CR-1305, National Aeronautics and Space Administration, Washington, D. C., March 1969.

9. Frandsen, J. D. and Marcus, H. L. "Crack Growth and Fracture in Gaseous Hydrogen," Effect of Hydrogen on Behavior of Materials, eds. Thompson, A. and Bernstein, I. M. The Metallurgical Society of AIME, NY (1976) pp. 233-248.

10. Shewman, P. G. "Hydrogen Attack of Carbon Steel," Effect of Hydrogen on Behavior of Materials, eds. Thompson, A. and Bernstein, I. M. The Metallurgical Society of AIME, NY (1976) pp. 59-69.

11. Steels for Hydrogen Service at Elevated Temperatures and Pressures for Petroleum Refineries and Petrochemical Plants, API Publication 941, American Petroleum Institute; Division of Refining, New York, July (1970).

12. Johnson, H. H. "Hydrogen and the Integrity of Structural Alloys." The Hydrogen Economy Miami Energy (Theme) Conf., editor: Veziroglu, T., Permagon Press, NY (1974), pp. S5-13, S6-14.

13. Pressouyre, G. M. Met. Trans. A. 10A, 1571 (1979).

14. McNabb, A. and Foster, P. K. Trans. TMS-AIME, 227, 618 (1963).

15. Oriani, R. A. Acta Met., 18, 147 (1970).

16. Pressourye, G. M. "Trap Theory of Hydrogen Embrittlement." Acta Met., 28, 895 (1980).

17. Caskey, G. R. and Pillinger, W. L. Met. Trans. A, 6A, 467 (1975).

18. Crank, J. The Mathematics of Diffusion, second edition, Clarendon Press, Oxford, 1975.

19. Volkl, J. and Alefeld, G. Diffusion in Solids: Recent Developments, A. S. Howick and J. J. Burton, Ed., pp. 231-305, Academic Press, N. Y., 1975.

20. Gonzalez, O. D. Trans. TMS-AIME, 245, 607 (1969).

21. Darken, L. S. and Smith, R. P. Corrosion, 5, 1 (1949).

22. Johnson, H. H., Quick, N. R. and Kumnick, A. J. Scripta Met., 13, 67 (1979).

23. Iino, M. Acta Met., 30, 367 (1982).

24. Pressouyre, G. M. and Bernstein, I. M. Met. Trans., 9A, 1571 (1978).

25. Lin, Ruey-Way. Ph.D. Thesis. Cornell University (1981).

26. Lacombe, P., Asaoka, T., Lapasset, G., Acouturier, M. Corrosion, 34, 39 (1978).

27. Bernstein, I. M. Scripta Met., 8, 343 (1974).

28. Gibala, R. Trans. AIME, 239, 1574 (1967).

29. Kumnick, A. J. and Johnson, H. H. Met. Trans., 5, 1199 (1974).

30. Evans, G. M. and Rollason, E. C. J. Iron Steel Inst., 207, 1484 (1969).

31. Kumnick, A. J. and Johnson, H. H. Acta Met., 28, 33 (1980).

32. Xie, S. X. and Hirth, J. P. Corrosion, 38, No. 9, 486 (1982).

33. Robertson, W. and Thompson, A. Met. Trans., 11A, 553 (1980).

34. Atrens, A., Mezzanotte, D., Fiore, N. and Genshaw, M. Cor. Sci., 20, 673 (1980).

35. Devanathan, M. and Stachurski, F. Proc. Royal Soc., 270A, 90 (1962).

36. Atrens, A., Mezzanotte, D., Fiore, N. F., and Genshaw, M. A. Cor. Sci., 20, 673 (1980).

37. Pourbaix, M. Atlas of Electrochemical Equilibria, NACE, Houston (1974).

38. Surkein, M. M.S. Thesis. University of Rhode Island, 1979.

39. Murali, J. Ph.D. Thesis. Virginia Polytechnic Institute and State University, August, 1980.

40. Bockris, J., McBreen, J. and Nanis, L. J. Electrochem. Soc., 112, 1025 (1965).

41. Namboodhiri, T. and Nanis, L. Acta Met., 21, 663 (1973).

42. Van Black, L. Elements of Materials Science and Engineering, Addison-Wesley, Mass. (1980), pp. 122.

43. R. Heidersbach, J. Jones and M. Surkein, Proc. of Second International Congress on Hydrogen in Metals, paper, 4A3, Paris, France, June 1977.

44. Choi, J. Y. Met. Trans., 1, 911 (1970).

45. Hirth, J. P. and Carnahan, B. Acta Met. 26, 1795 (1978).

APPENDIX A

DATA ANALYSIS

The value of lattice diffusivity used for data analysis is based on Equation 6 and is given by:

$$D = 3.1 \times 10^{-5} \text{ cm}^2/\text{sec at } 24^{\circ}\text{C} \tag{33}$$

The value of the effective diffusivity, D_{eff}, was calculated by two methods. The first method was the Laplace technique (36) given by the relation:

(for the rise transient case)

$$\frac{J_{\tau}}{J_{\infty}} = \frac{I_{\tau}}{I_{\infty}} = 1 - 2 \exp(-\pi^2 \tau) \tag{34}$$

τ = normalized time ($\tau = Dt/L^2$) (35)

J_{τ}, I_{τ} = the hydrogen flux or permeation current corresponding to the dimensionless parameter , respectively.

$J_{\infty} = I_{\infty}$ = the steady state hydrogen flux or permeation current, respectively.

The procedure used in this study to obtain D_{eff} values is as follows:

1. The experimental rise or decay currents are normalized and these values are plotted versus on a logarithmetic scale.
2. The experimental transients are then shifted along the abscissa by an amount log B until the experimental data points were coincident with the theoretical curve. Under these conditions

$$\log \tau = \log D/L^2 + \log t. \tag{36}$$

Using this technique (36) of fitting experimental data to the theoretical curve, it is possible to obtain an average value of D_{eff} for the whole experimental curve or values of D_{eff} appropriate to various parts of the curve. See Figure 21 for an illustration of this technique.

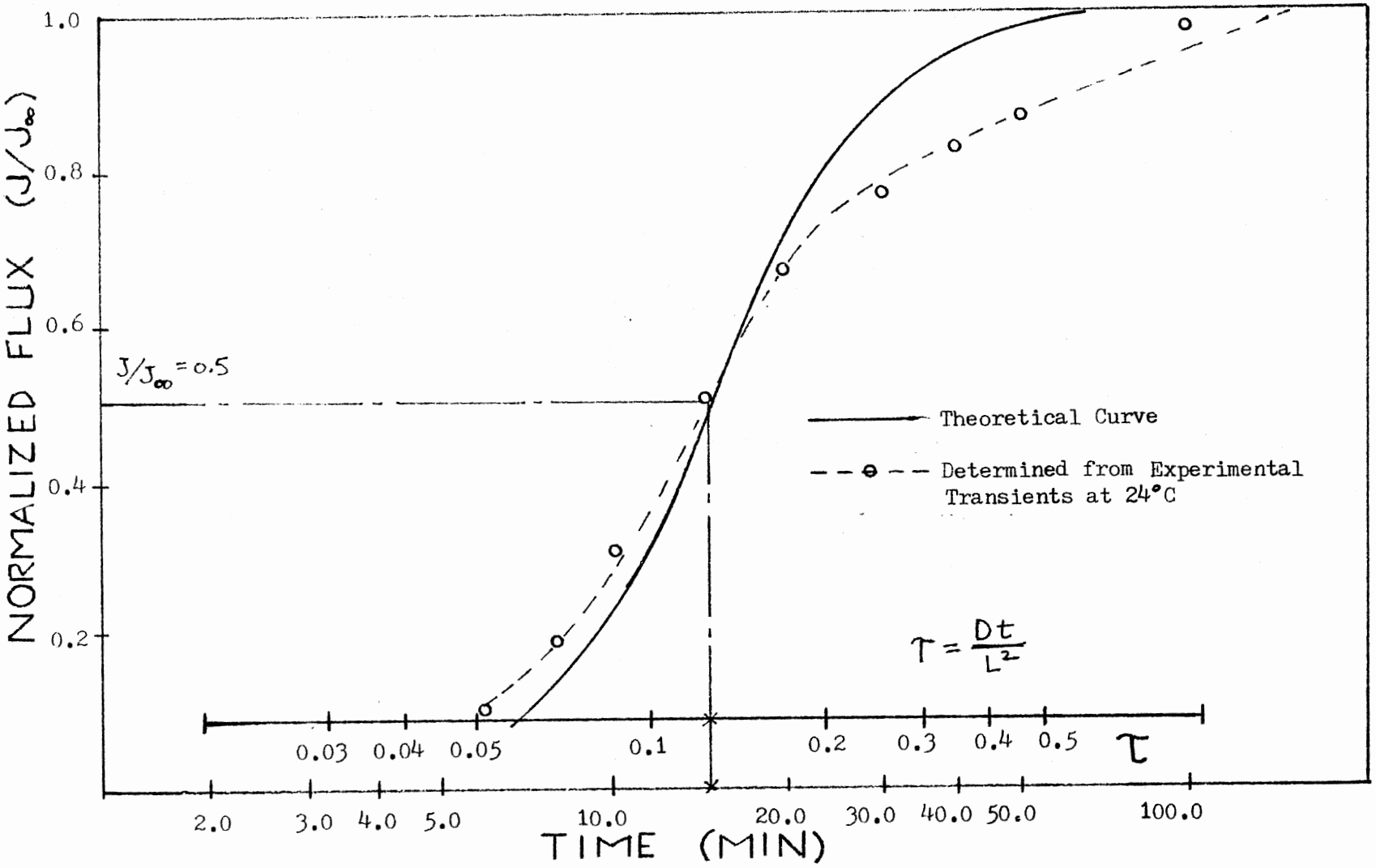

Figure 21. Theoretical Rise Transient Superimposed on Typical Experimental Data. (This Figure also Illustrates the Method of Fitting Experimental Data to the Theoretical Curves.)

The second method used to calculate D_{eff} is the time lag method (35) given by:

$$D = \frac{L^2}{6T_{lag}} \tag{37}$$

where

D = effective diffusivity

T_{lag} = time at which the rate of permeation is 0.63 times the steady-state value.

L = specimen thickness

From Fick's first law and Faraday's law of electrolysis, the permeation current density, I, can be expressed as hydrogen flux, J_∞, by the following relation:

$$I = -n\ F\ D \frac{\partial c}{\partial x} \tag{38}$$

where

c = concentration, mol cm^{-3}

n = number of electrons involved in the oxidation of hydrogen, eg. mol^{-1}

F = Faraday constant, 96,500 coul. (gm. eg.)

D = diffusion coefficient, cm^2/sec

The result of Equation 34 is:

$$10^{-6}\ amp/cm^2 = 1.25 \times 10^{13}\ atoms\ H/cm^2 sec = 1.04 \times 10^{11}\ moles\ H/cm^2 sec \tag{39}$$

Using Fick's first law again and Equation for J_∞, the hydrogen lattice concentration at the entry side of the membrane was determined from:

$$C_o = \frac{J_\infty\ L}{D_{eff}} \tag{40}$$

The permeability, ϕ, can be found from steady state permeation flux, J_∞, and specimen thickness, L, by the simple expression:

$$\phi = J_\infty L \tag{41}$$

Computer Program

The computer program listing used in this study is given in Appendix B. This program is based on the numerical solution to the McNabb-Foster equations (18). Caskey and Pillinger (23) have developed a finite difference method to solve the McNabb-Foster equations and this program is based on their approach. The McNabb-Foster equations are converted to dimensionless form and given as:

$$\frac{\partial u}{\partial \tau} + \frac{\partial w}{\partial \tau} = \frac{\partial^2 u}{\partial X^2} \tag{42}$$

$$\frac{\partial w}{\partial \tau} = \lambda u - \mu w - \nu uw \tag{43}$$

For the case of one dimensional diffusion, the variables can be defined as follows:

u = relative concentration = C/C_o

where C is the relative concentration of diffusant (# of species/cm^3 at X), and C_o is the surface concentration.

w = relative trapped concentration = nN/C_o

where N is the number of traps/cm^3, and n is the fraction occupied.

τ = reduced time = Dt/a^2

where X is the distance from the specimen surface. The parameters λ, μ, ν describe the rate at which atoms are captured and released from the traps and are defined as:

$$\lambda = N\ a^2/D \tag{44}$$

$$\mu = pa^2/D \tag{45}$$

$$\nu = C_o k a^2 / D \tag{46}$$

where k is the rate of capture of diffusing atoms in a volume $kXn(1-n)\delta V$ and p is the rate of release in the volume $pnN\delta V$.

The differential equations are solved with boundary conditions defined as:

$$U(o,t) = U_o^n = \text{constant} \tag{47}$$

$$U(1,t) = UM^n = 0 \tag{48}$$

$$W(o,t) = w_o^n = \text{constant} \tag{49}$$

$$W(1,t) = W_M^n = 0 \tag{50}$$

where

U_1^0, U_2^0, ... U^0_{M-1} and W_1^0, W_2^0, ... W^0_{M-1} are initial values.

Equations 10 and 11 are rewritten in finite difference form. The Crank-Nicolson forward and central difference method (18) gives the following:

$$\frac{U_m^{n+1} - U_m^n}{\Delta\tau} + \frac{W_m^{n+1} - W_m^n}{\Delta\tau} = \tfrac{1}{2}\left(\frac{U_{m+1}^{n+1} - 2U_m^{n+1} + U_{m-1}^{n+1}}{(\Delta X)^2}\right)$$

and

$$+ \tfrac{1}{2}\left[U_{m+1}^n - 2U_m^n + U_{m-1}^n\right] / \Delta x^2 \tag{51}$$

$$q_m/\Delta\tau = \tfrac{1}{2}\left[\lambda u_m^{n+1} - \mu W_m^{n+1} - \nu u_m^{n+1} W_m^{n+1}\right] \tag{52}$$

$$+ \tfrac{1}{2}\left[\lambda U_m^n - \mu W_m^n - \nu U_m^n W_m^n\right] \tag{53}$$

The system of resulting equations can be solved by the tridiagonal matrix method (18). Convergence and accuracy of the solutions depends on the ratio of $\Delta t/\Delta x^2$. When this ratio is lower than 2, there is convergence

of the solution (17).

The computer analysis technique consists of fitting the curve of the theoretical model to the experimental curve. The parameters, λ , μ and ν control the general nature of the diffusion equations and these parameters are selected so as to provide the proper fit between the two curves. Once these parameters are known, it is possible to determine other parameters such as k, p, N.

APPENDIX B

COMPUTER PROGRAM LISTING

COMPUTER PROGRAM LISTING

```
L
00010 //U11751A  JOB (11751,123-45-6789),'LOUT',TIME=(0,40),CLASS=A,
00020 // MSGCLASS=X,NOTIFY=U11751A
00030 /*PASSWORD LOUT
00040 //  EXEC  WATFIV
00050 //WATFIV.SYSIN DD *
00054 $JOB              ,TIME(0,40)
00060       DIMENSION A(100),B(100),C(100),D(100),P(100),U(100),W(100),
00070      $  X(100),R(100),S(100),Q(100),T(10000),F(10000),FC(44),TA(10
0)
00080       REAL LT,LAM,MU,NU
00090       LAM=1.0E8
00100       MU=3.0E5
00110       NU=7.0E3
00120       DIFF=3.1E-5
00130       LT=0.02
00140       TH=0.5
00150       N=10
00160       N1=N-1
00170       RATIO=2.0
00180       DELX=1./FLOAT(N-1)
00190       DX=DELX*LT
00200       DELTAU=RATIO*(DELX**2)
00210       TDELT=DELTAU*(LT**2)/(DIFF*60.0)
00220       DATA U/100*0.0/, W/100*0.0/
00230 C     BOUNDARY CONDITIONS
00235       U(1)=10.0
00240       U(N)=0.0
00250 C     INITIALIZE TIME VALUES
00251       J=0
00254       WRITE(6,100)
00256 100   FORMAT( '1',///'------------------- INPUT PARAMETERS -------
----',
00257      $ '----------'/)
00258       WRITE(6,200)LT,DIFF,LAM,MU,NU,RATIO,DELX,DELTAU,TDELT,U(1),U
(N)
00260 200   FORMAT(/// SPECIMEN THICKNESS= ',F10.4,' CM'/
00262      $ ' DIFFUSION COEF.= ', E10.4,' CM**2/SEC'/
00264      $ ' LAM= ', E10.4,' MU= ',E10.4,' NU= ',E10.4/
00266      $ ' RATIO= ',F10.4, '  DELX=', F10.4,' DELTAU= ',F10.4/
00268      $ ' TDELT= ',F10.4,'  MINUTES'/
00270      $ ' ENTRANCE SIDE CONCENTRATION= ',F10.4/
00272      $ ' EXIT SIDE CONCENTRATION     = ',F10.4//)
00279       T(1)=0.0
00280       TFINAL=20.0
00290 5     J=J+1
00300       T(J+1)=T(J)+TDELT
00310       DATA A/100*-0.5/, B/100*0.0/, C/100*-0.5/, D/100*0.0/,
00320      $  P/100*0.0/, R/100*0.0/, S/100*0.0/
00330       U(1)=10.0
00340       DO 90 I=1,N
00350       DN=TH*(MU+(NU*U(I)))+(1.0/DELTAU)
00360       R(I)=TH*(LAM-(NU*W(I)))/DN
00370       B(I)=(((DELX**2.0)/DELTAU)*(1.0+R(I)))+(2.0*TH)
00380       S(I)=((LAM*U(I))-(MU*W(I))-(NU*U(I)*W(I)))/DN
00390 90    CONTINUE
00400       DO 20 I=2,N1
00410       D(I)=U(I+1)-(2.0*U(I))+(U(I-1))-((S(I)*(DELX**2.0))/DELTAU)
00420 20    CONTINUE
00430       CALL TRID(A,B,C,D,P,N)
00440       DO 95 I=2,N1
00450       U(I)=U(I)+P(I)
00460 95    CONTINUE
00470       DO 96 I=1,N
00480       Q(I)=(R(I)*P(I))+S(I)
00490       W(I)=Q(I)+W(I)
00500 96    CONTINUE
00519       F(J)=(U(N-1)+W(N-1))/DX
00520       IF(T(J)-TFINAL)5,800,800
00521 800    WRITE(6,111)T(J+1)
00522 111   FORMAT(////'  TIME=  ,F12.7,'MINUTES'//'  RELATIVE CONCENTRA
TION'/
```

COMPUTER PROGRAM LISTING

```
00523       $ )
00524         WRITE(6,222)(U(I),I=1,N)
00525 222    FORMAT(10(2X,F12.4))
00526         WRITE(6,333)
00527 333    FORMAT(///'  TRAPPED CONCENTRATION'/)
00528         WRITE(6,444)(W(I),I=1,N)
00529 444    FORMAT(10(2X,F12.4))
00530         WRITE(6,888)
00531 888    FORMAT(//////'    NORMALIZED TIME   NORMALIZED FLUX'/)
00532         DO 900 I=1,J
00533         F(I)=F(I)/F(J)
00534 900    T(I+1)=(T(I+1)*DIFF*60.)/LT**2
00535         WRITE(6,666)(T(I+1),F(I),I=1,J,50)
00540 666    FORMAT(3X,F14.7,3X,F14.7)
00550         DATA PC/0.,0.,0.,0.,0.,10.5,36.8,68.,95.,126.,147.,173.,194.
,212.,
00560       $ 231.,241.5,257.,265.,278.,288.8,294.,304.5,315.,336.,357.,3
78.,
00570       $ 389.,399.,406.9,409.5,412.,417.,420.,431.,441.,446.,449.,
00580       $ 451.5,453.,454.,459.,462.,467.,472./
00590         NN=44
00600         DO 30 I=1,22
00610         TA(I)=FLOAT(I*2)
00620   30    CONTINUE
00630         DO 40 I=1,NN
00640         PC(I)=PC(I)/47.2
00650 40      CONTINUE

00660         DO 50 I=23,44
00670         TA(I)=TA(I-1)+4.
00680 50      CONTINUE
00690         STOP
00700         END
00710         SUBROUTINE TRID(AA,BB,CC,DD,PP,N)
00720         DIMENSION AA(50),BB(50),CC(50),DD(50),PP(50)
00730         INTEGER N,N1
00740         N1=N-1
00750         N2=N-2
00760         DO 33 I=3,N1
00770         S=AA(I)/BB(I-1)
00780         BB(I)=BB(I)-(S*CC(I-1))
00790         DD(I)=DD(I)-(S*DD(I-1))
00800 33      CONTINUE
00810         PP(N1)=DD(N1)/BB(N1)
00820         DO 44 I=2,N2
00830         J=N1-I+1
00840         PP(J)=(DD(J)-(CC(J)*PP(J+1)))/BB(J)
00850 44      CONTINUE
00860         RETURN
00870         END
00880 $ENTRY
00890 $IBSYS
00900 /*
END OF DATA
```

COMPUTER OUTPUT DATA FOR ANNEALED ARMCO IRON

INPUT PARAMETERS

SPECIMEN THICKNESS= 0.0130 CM
DIFFUSION COEF.= 0.3100E-04 CM**2/SEC
LAM= 3.1500E 04 MU= 0.3000E 03 NU= 3.4000E 02
RATIO= 2.0000 DELX= 0.1111 DELTAU= 0.0247
TDELT= 0.0043 MINUTES
ENTRANCE SIDE CONCENTRATION= 10.0000
EXIT SIDE CONCENTRATION = 0.0000

TIME= 2.0066000MINUTES

RELATIVE CONCENTRATION

10.0000000 8.8888480 7.7777760 6.6666480 5.5555450 4.4444250 3.3333210 2.2222130 1.1111050 0.0000000

TRAPPED CONCENTRATION

21.4286700 20.3389700 19.2503800 17.6470300 15.9574100 13.9534600 11.5384300 8.5714060 4.8286950 0.0000000

NORMALIZED TIME	NORMALIZED FLUX
0.0246913	0.0030036
0.1481480	0.0052437
0.2716047	0.0670763
0.3950613	0.2201435
0.5185180	0.4092333
0.6419746	0.5782639
0.7654309	0.7081702
0.8888880	0.8012466
1.0123430	0.8657680
1.1358010	0.9097697
1.2592580	0.9395182
1.3827140	0.9595105
1.5061710	0.9729519
1.6296270	0.9819359
1.7530850	0.9879411
1.8765410	0.9919536
1.9999980	0.9946320
2.1234540	0.9964195
2.2469110	0.9976120
2.3703680	0.9984075
2.4938240	0.9989381
2.6172810	0.9992920
2.7407370	0.9995279
2.8641940	0.9996852
2.9876500	0.9997903
3.1111070	0.9998603
3.2345640	0.9999070
3.3580210	0.9999380
3.4814780	0.9999585
3.6049350	0.9999722
3.7283890	0.9999815
3.8518460	0.9999880
3.9753030	0.9999921
4.0987590	0.9999949
4.2222160	0.9999966
4.3456740	0.9999977
4.4691310	0.9999986
4.5925870	0.9999993

4.7160440	0.9999996	
4.8395010	1.0000000	
4.9629580	1.0000000	
5.0864150	1.0000000	
5.2098720	1.0000000	
5.3333290	1.0000000	
5.4567860	1.0000000	
5.5802420	1.0000000	
5.7036990	1.0000000	
5.8271560	1.0000000	
5.9506110	1.0000000	
6.0740680	1.0000000	
6.1975240	1.0000000	
6.3209810	1.0000000	
6.4444370	1.0000000	
6.5678940	1.0000000	
6.6913510	1.0000000	
6.8148080	1.0000000	
6.9382650	1.0000000	
7.0617220	1.0000000	
7.1851780	1.0000000	
7.3086360	1.0000000	
7.4320920	1.0000000	
7.5555500	1.0000000	
7.6790060	1.0000000	
7.8024630	1.0000000	
7.9259200	1.0000000	
8.0493770	1.0000000	
8.1728310	1.0000000	
8.2962880	1.0000000	
8.4197450	1.0000000	
8.5432020	1.0000000	
8.6666590	1.0000000	
8.7901150	1.0000000	
8.9135720	0.9999998	
9.0370290	1.0000000	
9.1604870	1.0000000	
9.2839430	1.0000000	
9.4074000	1.0000000	
9.5308570	1.0000000	
9.6543140	1.0000000	
9.7777700	1.0000000	
9.9012270	1.0000000	

10.0246800	1.0000000
10.1481400	1.0000000
10.2715900	0.9999998
10.3950500	1.0000000
10.5185000	1.0000000
10.6419600	1.0000000
10.7654200	1.0000000
10.8888700	1.0000000
11.0123300	1.0000000
11.1357900	1.0000000
11.2592500	1.0000000
11.3827000	0.9999998
11.5061600	1.0000000

STATEMENTS EXECUTED= 9300

COMPUTER OUTPUT DATA FOR COLD WORKED ARMCO IRON

---------- INPUT PARAMETERS ----------

SPECIMEN THICKNESS= 0.0200 CM
DIFFUSION COEF.= 0.3100E-04 CM**2/SEC
LAM= 0.1000E+09 MU= 0.3000E+06 NU= 0.7000E+04
RATIO= 2.0000 DELX= 0.1111 DELTAU= 0.0247
TDELT= 0.0053 MINUTES
ENTRANCE SIDE CONCENTRATION= 10.0000
EXIT SIDE CONCENTRATION = 0.0

TIME= 20.0099487MINUTES

RELATIVE CONCENTRATION

10.00	8.80	7.62	6.45	5.30	4.16	3.10	2.05	1.02	0.0

TRAPPED CONCENTRATION

3219.58	2434.48	2155.63	1867.70	1572.29	1270.78	963.88	651.25	331.10	0.0

NORMALIZED TIME	NORMALIZED FLUX
0.0246913	0.0000000
1.2592535	0.0000000
2.4938135	0.0000016
3.7283764	0.0000251
4.9629078	0.0001559
6.1972570	0.0005901
7.4316235	0.0014785
8.6659908	0.0036928
9.9003553	0.0071552
11.1347208	0.0123908
12.3690872	0.0196806
13.6034536	0.0292019
14.8378201	0.0410256
16.0721893	0.0551255
17.3065491	0.0713955
18.5409241	0.0896696
19.7752838	0.1097396
21.0096588	0.1313730
22.2440186	0.1543273
23.4783936	0.1783603
24.7127686	0.2032378
25.9471283	0.2287408
27.1814880	0.2546684
28.4158630	0.2808384
29.6502228	0.3070890
30.8845978	0.3332779
32.1189728	0.3592824
33.3533325	0.3849958
34.5877075	0.4103308
35.8220673	0.4352146
37.0564270	0.4595875
38.2907867	0.4834022
39.5251617	0.5066198
40.7595367	0.5292121
41.9939117	0.5511588
43.2282410	0.5724455
44.4626160	0.5930648
45.6969910	0.6130130
46.9313812	0.6322920
48.1657104	0.6509066
49.4000854	0.6688632
50.6344604	0.6861726
51.8688354	0.7028467
53.1032104	0.7188990
54.3375549	0.7343436
55.5719299	0.7491969
56.8063049	0.7634744
58.0406799	0.7771881
59.2750244	0.7903532
60.5093994	0.8029997
61.7437744	0.8151411
62.9781494	0.8267915
64.2125244	0.8379718
65.4468689	0.8486946
66.6812439	0.8589780
67.9156189	0.8688377
69.1499939	0.8782905
74.0874634	0.9123250
75.3192902	0.9199611
76.5503387	0.9272757
77.7813721	0.9342808
79.0124207	0.9409924
80.2434540	0.9474187
81.4745026	0.9535716
82.7055359	0.9594626
83.9365845	0.9651040
85.1676025	0.9705033
86.3986664	0.9756738
87.6297302	0.9806235
88.8607483	0.9853603
90.0918121	0.9898952
91.3228302	0.9942344
92.5538798	0.9983878

VITA

Steven Edward Charles Maschino

Candidate for the Degree of

Master of Science

Thesis: DIFFUSION OF HYDROGEN IN IRON IN STEEL

Major Field: Mechanical Engineering

Biographical:

Personal Data: Born in Oklahoma City, Oklahoma, November 8, 1955, the son of Mr. and Mrs. Edward Maschino.

Education: Graduated from Mustang High School, Mustang, Oklahoma, in May, 1974; received Bachelor of Science in Mechanical Engineering degree from Oklahoma State University, in May, 1981; completed requirements for Master of Science degree in Mechanical Engineering in December, 1982.

Professional Experience: Design Engineer, Benham and Blair Associates, Summer work 1979-1980. Graduate teaching assistant, Oklahoma State University, School of Mechanical Engineering, 1981-1982.